

We are IntechOpen, the world's leading publisher of Open Access books Built by scientists, for scientists

6,900

Open access books available

185,000

International authors and editors

200M

Downloads

Our authors are among the

154

Countries delivered to

TOP 1%

most cited scientists

12.2%

Contributors from top 500 universities



WEB OF SCIENCE™

Selection of our books indexed in the Book Citation Index
in Web of Science™ Core Collection (BKCI)

Interested in publishing with us?
Contact book.department@intechopen.com

Numbers displayed above are based on latest data collected.
For more information visit www.intechopen.com



Thermoelectric Power in Graphene

N.S. Sankeshwar, S.S. Kubakaddi and B.G. Mulimani

Additional information is available at the end of the chapter

1. Introduction

Recent years have witnessed considerable interest devoted to the electronic properties of graphene [1-3]. Graphene, a one-atom-thick sheet of carbon atoms arranged in a honeycomb crystal, exhibits unique properties like high thermal conductivity, high electron mobility and optical transparency, and has the potential for use in nano-electronic and optoelectronic devices. With the size of these devices shrinking through integration, thermal management assumes increasingly high priority, prompting the study of thermoelectric effects in graphene systems.

The thermoelectric (TE) effect refers to phenomena by which either a temperature difference creates an electric potential or an electric potential creates a temperature difference. An interesting transport property, thermoelectric power (TEP) has been a source of information to physicists for over a century [4]. TE devices are used as generators and coolers to convert thermal energy into electrical energy or *vice versa*. The potential of a material for TE applications — solid state refrigeration and power generation — generally is determined in large part by a measure of the material's TE figure of merit, $ZT = S^2 \sigma T / \kappa$, where S is the thermoelectric power (also called Seebeck coefficient), σ the electrical conductivity, and κ the thermal conductivity of the material. Efficient TE energy conversion, therefore, requires materials that have an enhanced power factor $S^2 \sigma$ and reduced κ [4, 5]. The state of art TE materials possess a value $ZT \sim 1$, at room temperature [4, 5]. There is no well-defined theoretical limit to ZT . Values of $ZT \sim 2-3$ would make TE refrigeration competitive with vapour compression refrigeration systems [4, 5]. Even a modest increase in value of ZT would, therefore, provide important opportunities for applications [6]. Recent studies indicate that ZT could be increased nearly fourfold, by optimizing the potential of graphene systems [7].

The interest in the TEP of a material system stems not only from its relation to ZT but also due to its sensitivity to the composition and structure of the system and to the external

fields. The TE effect has been able to shed much light on the interaction of electrons and phonons, impurities and other defects. Further, the three transport parameters S , σ and κ are not independent of each other. The Seebeck coefficient, for instance, is partially determined by the electrical conductivity. This provides a challenge for theoreticians and experimentalists alike to search for ways to increase its value. An optimization, say, of the Seebeck coefficient for any material will involve understanding and appropriately modifying its electronic properties. Conventional thermocouples, made from metal or metal alloys, generate Seebeck voltages typically tens of microvolts per Kelvin [8, 9]. Those made from semiconductors with tailored material properties [10] and geometry [11, 12] possess voltages of a few hundreds of microvolts per Kelvin. One of the objectives, therefore, of studies in TEs has been to search for materials with optimized electronic band structures [13] and thermal properties [14, 15]. Much of the recent renewed interest in TEs has been stimulated by the prospect that graphene, with its unique electrical and thermal properties, could provide increased figure of merit.

Ever since its discovery, great interest has been evinced in the electronic properties of graphene [1-3]. Graphene also exhibits interesting TE effects. For instance, compared to elemental semiconductors, it has higher TEP and can be made to change sign by varying the gate bias [16-18]. The unique properties, including high mechanical stiffness and strength, coupled with high electrical and thermal conductivity, make graphene an exciting prospect for a host of future applications in nanoelectronics, thermal management and energy storage devices (For reviews on graphene physics, see [2] and [3]). Technical advances have now made possible the realization of tailor-made 2D graphene systems, such as single-layer graphene (SLG), bilayer graphene (BLG), graphene nanoribbon (GNR), graphene dots, graphene superlattices and defected graphene. Most of the experimental and theoretical work has concerned the electrical and thermal conductivity of such systems. (For a review on recent progress in graphene research, see [19]). However, in the recent past, a good amount of literature has accumulated on the TE properties of graphene systems, and a coherent picture is just emerging into understanding TE effect in graphene.

The present work addresses one of the important components of TE transport in graphene, namely, TEP, also referred to, simply, as thermopower. TEP has been a powerful tool for probing carrier transport in metals and semiconductors [8-12]. Being sensitive to the composition and structure of a system, it is known to provide information complementary to that of resistivity (or conductivity), which alone is inadequate, say, in distinguishing different scattering mechanisms operative in a system.

In this chapter, we review the literature on TEP in graphene systems and present its understanding using the semi-classical Boltzmann transport theory. In Section 1, the electronic structures and phonon dispersion relations for SLG, BLG and GNR systems are described. In the next section, besides a survey of the experimental work, the basic theory of TEP in 2D systems is given, and its relation with other TE transport coefficients is discussed. In Section 3, the diffusion contribution to TEP of graphene systems is discussed. Section 4 deals with the phonon-drag contribution to TEP. An analysis of the experimental data, in terms of the

diffusion and drag components, is also presented. This is followed by a summary of the chapter.

1.1. Graphene systems

A single-layer graphene, commonly referred to simply as graphene, is one of the recent nanomaterials. It is a monolayer of graphite with a thickness of 0.34 nm, consisting of carbon atoms in the sp^2 hybridization state, with the three nearest-neighbour carbon atoms in the honeycomb lattice forming σ bonds. The carriers in graphene are confined in this 2D layer [2, 3].

The 2D honeycomb structure of graphene lattice with two equivalent lattice sites, A and B (Figure 1.(a)), can be thought of as a triangular lattice with a basis of two atoms per unit cell, with 2D lattice vectors $\mathbf{a}_1 = (a/2)(3, \sqrt{3})$ and $\mathbf{a}_2 = (a/2)(3, -\sqrt{3})$, where $a = 0.142$ nm is the C-C distance. The inequivalent corners $\mathbf{K} = (2\pi/a)(1/3, 1/3\sqrt{3})$ and $\mathbf{K}' = (2\pi/a)(1/3, -1/3\sqrt{3})$ of the Brillouin zone are called Dirac points. The existence of the two Dirac points, K and K', where the Dirac cones for electrons and holes touch each other in momentum space (Figure 1.(b)), gives rise to a valley degeneracy, $g_v = 2$. Graphene is a zero band-gap semiconductor with linear long-wavelength energy dispersion for both electrons and holes in the conduction and valence bands. The two equivalent lattice sites make carrier transport interesting giving rise to the 'chirality' in its carrier dynamics [3]. The thermoelectric transport properties of graphene, discussed in this chapter, follow from the linear low-energy dispersion and the chiral character of the bands.

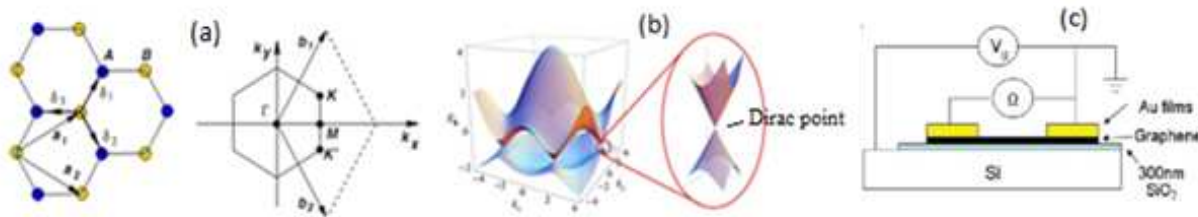


Figure 1. (a) Graphene honeycomb lattice and the Brillouin zone. The two sublattices are shown in different colours. (b) Graphene band structure. An enlargement close to the K and K' point shows Dirac cones. (from [2]) (c) Typical configuration for gated graphene.

Gapless graphene has a charge neutrality point (CNP), that is, the Dirac point, where its character changes from being electron-like to being hole-like. For pure graphene the Fermi surface is at the Dirac point. The system with no free carriers at $T = 0$ K and E_F at the Dirac point is called intrinsic graphene. It has a completely filled valence band and an empty conduction band. However, any infinitesimal doping, as also any finite temperature, with electrons present in the conduction band, makes the system 'extrinsic'. It is possible experimentally, by varying the external gate voltage, to tune the system from being electron-like to being hole-like, with the system going through its intrinsic nature at the CNP [3]. In the case

of a gapped system with an insulating region in between, one may not access the intrinsic nature of graphene.

The electronic properties of graphene depend on the number of layers. Generally, the graphene community distinguishes between single-layer, bilayer and few-layer graphene, the latter of which refers to graphene with a layer number less than ten. Bilayer graphene (BLG) consists of two graphene monolayers weakly coupled by interlayer carbon hopping, which depends on the manner of stacking of the two layers with respect to each other; typically they are arranged in A-B stacking arrangement. The bilayer structure, with the various electronic hopping energy parameters γ_i , is shown in Figure 2.(a). The low energy, long wavelength electronic structure of BLG for A-B stacking of the two layers is depicted in Table 1. It may be noted that unbiased BLG is gapless. However, by applying an external voltage, a semiconducting gap can be induced in the otherwise zero-gap band structure [3].

In order to improve applicability, graphene needs to acquire a bandgap. This can be achieved by appropriate patterning of the graphene sheet into nanoribbons. A graphene nanoribbon (GNR) is a quasi-one-dimensional (Q1D) system that confines the graphene electrons in a thin strip of (large) length L and a finite (small, a few nm) width W . Figure 2. (b) shows a honeycomb lattice of a GNR having zigzag edges along the x-direction and armchair edges along the y-direction. The resulting confinement gap, E_g , depends on the chirality of the edges (armchair or zigzag) and the width of the ribbon. Choosing a GNR to be macroscopically large say along the y-direction but finite along the x-direction, gives a GNR with armchair edges (AGNR), and, conversely, a GNR chosen with width along y-direction gives a zigzag terminated GNR (ZGNR). A ZGNR is metallic in nature, whereas an AGNR can be metallic or semiconducting, with E_g inversely proportional to W [3, 20].

One of the strategies adopted to achieve higher mobility in graphene samples is to improve the substrate quality or eliminate the substrate altogether by suspending graphene over a trench. Improved growth techniques have enabled obtaining graphene as a suspended membrane, supported only by a scaffold or bridging micrometer-scale gaps schematic of which is shown in Figure 2.(c). Suspended graphene (SG), shows great promise for use in nanoelectronic devices. With most of the impurities limiting electron transport sticking to the graphene sheet and not buried in the substrate, a large reduction in carrier scattering is reported [21] in current-annealed SG samples. However, unlike supported graphene, only a small gate voltage ($V_g \sim 5$ V) can be applied to a SG sample before it could buckle and bind to the bottom of the trench. Despite limited carrier densities, Bolotin *et al* [22] report a mobility of $1.7 \times 10^5 \text{ cm}^2 \text{V}^{-1} \text{s}^{-1}$ in ultra-clean SG with $n_s \sim 2 \times 10^{15} \text{ m}^{-2}$. The electronic properties of SG can be affected by strain. The layer(s) may be under strain either due to the electrostatic force arising from the gate or as a result of micro-fabrication, or even by applying strain in a controlled way. Recent studies suggest that strain can be used to engineer graphene electronic states [23] and hence the transport properties.

In the following, the thermoelectric property of TEP will be reviewed with regard to the three systems, namely SLG, BLG and AGNR.

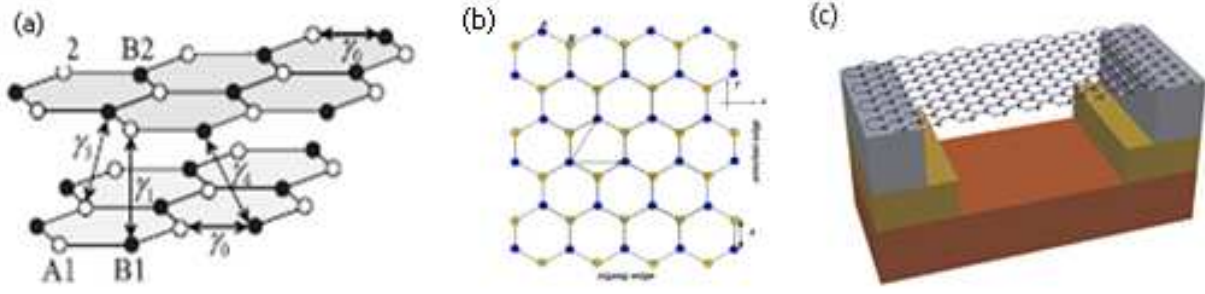


Figure 2. Lattice structure of (a) BLG, and (b) GNR. (from [2]). (c) Schematic of suspended SLG.

1.2. Electronic structures

1.2.1. Single layer graphene

The transport characteristics of a material are intimately related to the energy band structure. The carriers in the graphene lattice are free to move in two dimensions. In the carrier transport of graphene, the carriers — electrons and holes — close to the Dirac points are of importance. Their transport is described by a Dirac-like equation for massless particles [2, 3]:

$$-i\hbar v_F \boldsymbol{\sigma} \cdot \nabla \psi(r) = E \psi(r) \quad (1)$$

where $\boldsymbol{\sigma} = (\sigma_x, \sigma_y)$ is the vector of Pauli matrices in 2D and $\psi(\mathbf{r})$ includes a 2D plane wave and a spinor (graphene pseudospin) function. In the continuum limit Eq. (1) corresponds to the effective low energy Dirac Hamiltonian

$$H(k) = \hbar v_F \begin{pmatrix} 0 & k_x - ik_y \\ k_x + ik_y & 0 \end{pmatrix} = \hbar v_F \boldsymbol{\sigma} \cdot \mathbf{k} \quad (2)$$

The electronic band structure of the energy (E) versus wavevector (\mathbf{k}) relation for the graphene carriers is given by the solution of (1). The solution of (1) has been calculated in the tight-binding model up to the next-nearest neighbor approximation [24]. The carrier wavefunctions, energy eigenvalues, the density of states and the low-energy (close to the CNP, K) band structure for SLG are given in Table 1 [2].

Being interested mostly in understanding electron transport for small energies and relatively small carrier concentrations, only the low- \mathbf{k} , linear dispersion aspects of the band structure are considered close to the K and K' points where the Dirac cones for electrons and holes touch each other (see Figure 1.b). SLG is thus a zero band-gap semiconductor with a linear, long-wavelength ($k \ll 2\pi/a$) energy dispersion for both electrons (in the conduction band) and holes (in the valence band) with the conduction and valence bands intersecting at $\mathbf{k} = 0$ [2, 3]:

$$E_k = s \hbar v_F |k| \quad (3)$$

Here, $s = +1$ (-1) corresponds to the conduction (valence) band, $\mathbf{k} = i k_x + j k_y$ denotes the carrier wavevector measured from the relevant Dirac point, and $v_F = 3ta/2\hbar$, a constant, is called the graphene (Fermi) velocity; with the nearest-neighbor hopping amplitude, $t \sim 2.5$ eV, $v_F \sim 10^6$ ms⁻¹. The linearity of the dispersion relation signifies that the effective mass of charge carriers vanishes, and hence the interaction between electrons or holes and the 2D crystalline lattice is weak, and the charge carriers can propagate without collisions through graphene. Graphene can, therefore, be modeled as a 2D gas of massless fermions [3].

1.2.2. Bilayer graphene

The effective Hamiltonian for a BLG, in the low energy, long-wavelength regime is [3]

$$H(k) = -\frac{\hbar^2}{2m} \begin{pmatrix} 0 & (k_x - ik_y)^2 \\ (k_x + ik_y)^2 & 0 \end{pmatrix} \quad (4)$$

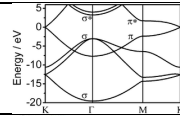
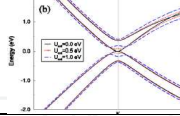
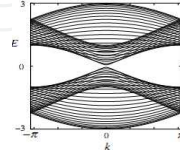
where m is the effective mass of the carriers. The electron wavefunctions and energy eigenvalues around the \mathbf{K} and \mathbf{K}' points at the corners of graphene Brillouin zone are given in Table 1 [25]. The BLG electronic structure, consisting of two branches, depends on the electrostatic potential, V , between the two layers. It controls an effective band-gap opening near Dirac point. For $V=0$, BLG is a gapless semiconductor with parabolic dispersion. The low-field electron transport is discussed with respect to the lowest branch.

1.2.3. Graphene nanoribbon

The spectrum of GNRs depends on the nature of their edges. The low-energy electronic states of GNRs near the two non-equivalent Dirac points (\mathbf{K} and \mathbf{K}') can be described by the 4x4 Dirac equation and using the appropriate boundary conditions. The effective Hamiltonian for a GNR is [26]

$$H(k) = \gamma \begin{pmatrix} 0 & (k_x - ik_y) & 0 & 0 \\ (k_x + ik_y) & 0 & 0 & 0 \\ 0 & 0 & 0 & (k_x + ik_y) \\ 0 & 0 & (k_x - ik_y) & 0 \end{pmatrix} \quad (5)$$

where $\gamma (= \sqrt{3}ta/2 = \hbar v_F/\sqrt{3})$ is a band parameter. The expressions for the electron wave functions, energy eigenvalues, density of states and the band structures for a AGNR (the system considered here) derived from admixing the states in the \mathbf{K} and \mathbf{K}' valleys and satisfying hard wall

System	Wavefunctions	Eigenvalues	Density of States	Band Structure
SLG	$\psi_{\pm,K}(r) = \frac{1}{\sqrt{2LW}} \begin{pmatrix} e^{-i\theta_k} \\ \pm 1 \end{pmatrix} e^{ik \cdot r}$	$E_k = \hbar v_F k $	$\rho(E_k) = \frac{2 E_k }{\pi(\hbar v_F)^2}$	
BLG	$\psi_{\pm,K}(r) = \frac{1}{\sqrt{2LW}} \begin{pmatrix} e^{-2i\theta_k} \\ \pm 1 \end{pmatrix} e^{ik \cdot r}$	$E_k = \frac{\hbar^2 k^2}{2m}$	$\rho(E_k) = \frac{2m}{\pi \hbar^2}$	
AGNR	$\Psi_{n,k_y}(\mathbf{r}) = \left[\psi_{n,k_y}(\mathbf{r}) - \psi'_{n,k_y}(\mathbf{r}) \right] / \sqrt{2}$ with $\psi_{n,k_y}(\mathbf{r}) = \sqrt{1/2LW} e^{i[(\Delta K/2) - k_n]x} \varphi_{n,k_y}(y)$ $\psi'_{n,k_y}(\mathbf{r}) = \sqrt{1/2LW} e^{-i[(\Delta K/2) - k_n]x} \varphi_{n,k_y}(y)$ $\varphi_{n,k_y}(y) = e^{ik_y y} \begin{pmatrix} 1 \\ -e^{-i\theta_{n,k_y}} \end{pmatrix}$	$E_{n,k_y} = \hbar v_F \sqrt{k_n^2 + k_y^2}$	$\rho(E_{n,k_y}) = \frac{2}{\pi \hbar v_F} \left[\frac{E_{n,k_y}}{\{E_{n,k_y}^2 - (E_n)^2\}^{1/2}} \right]$	

Meanings of symbols (Table 1.):

L : Length of graphene system; W : Width of graphene system; $\mathbf{r} \equiv (x, y)$: 2D electron position vector; $\mathbf{k} \equiv (k_x, k_y)$: 2D electron wavevector

v_F - Fermi velocity; m - Effective mass; $\theta_k = \tan^{-1}(k_x/k_y)$.

$E_n = \pm n \pi \hbar v_F / 3W$: AGNR subband energy; subband index, $n=1, 2, 4, 5, 7, 8, \dots$; $E_g = 2\pi \hbar v_F / 3W$ – Band gap

$k_n = \pm n\pi / 3W$: electron transverse wave vector; $\Delta K = 4\pi / 3a$, a – lattice constant; $\theta_{n,k_y} = \tan^{-1}(k_n/k_y)$.

Table 1. Electron wavefunctions, energy eigenvalues, density of states and band structures of graphene systems [2, 25, 27]

boundary conditions, are given in Table 1 [26, 27]. The confinement of electrons to a Q1D system gives rise to the subband structure with an energy gap at the Dirac point.

1.3. Phonon dispersion relations

Vibrations in the 2D graphene lattice are characterized by two types of acoustic phonons: those vibrating in the plane of layer with linear longitudinal and transverse acoustic branches (LA and TA), and those vibrating out of the plane of the layer – the so-called flexural phonons (ZA) [1-3].

The low-energy in-plane phonons have the usual linear dispersion relation

$$\omega_q = v_s q \quad (6)$$

where, $\mathbf{q} = (q_x, q_y)$ is the 2D phonon wavevector, and v_s denotes the velocity of the in-plane phonons of mode s ($\equiv L, T$). The group velocities $v_L = \sim 13.6 \times 10^3 \text{ ms}^{-1}$ and $v_T = \sim 21.3 \times 10^3 \text{ ms}^{-1}$ are larger than those in silicon.

The acoustic flexural phonons (FPs) are described by an approximately quadratic dispersion relation [1, 28]:

$$\omega_q \approx \alpha |q|^2 \quad (7)$$

with $\alpha = \sqrt{\kappa / \rho}$, κ being bending rigidity and ρ the mass density. Eq.(7) is applicable to the free-standing membranes as in suspended graphene (SG).

The existence and possible modification of the ZA modes, as in the case of SG membrane under tension, are known to lead to the unusual thermal transport in graphene [15]. For slowly varying finite in-plane stresses, the dispersion relation of the FPs is anisotropic. Assuming uniaxial strain \bar{u} , the effective dispersion relation of FPs, in the isotropic approximation, may be expressed as as [28]:

$$\omega_q = q \sqrt{\alpha^2 q^2 + \bar{u} v_L^2} \quad (8)$$

The quadratic dispersion relation (8) of FPs becomes linear at long wavelengths [28].

2. Thermoelectric power – Basics

Thomas Johann Seebeck observed that a conductor generates a voltage when subjected to a temperature gradient. This phenomenon is called Seebeck effect, and can be expressed as [4, 5, 8, 9, 11]

$$V = S \Delta T \quad (9)$$

where V is thermoelectric voltage, ΔT is temperature difference, and S is the Seebeck coefficient (see Figure 3). The Seebeck coefficient is also called thermoelectric power. One may define an ‘absolute’ thermopower characteristic of a particular material.

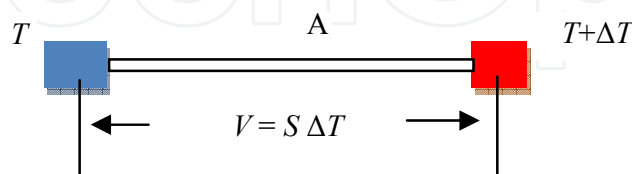


Figure 3. Seebeck effect. Material A cooled at one end (in blue color) with low temperature T and heated at the other end (red color) at higher temperature $T + \Delta T$, results in a voltage difference as a function of temperature difference (ΔT)

On the other hand, Jean Charles Peltier discovered that when an external voltage is applied, the resulting current flow is associated with a heat flow. The Peltier effect is thus the reverse

of the Seebeck effect — it refers to the temperature difference induced by voltage gradient. A third thermoelectric phenomenon, called the Thomson effect after its discoverer, William Thomson, is the reversible evolution (or absorption) of heat in a homogeneous conductor that carries an electric current and in which a temperature gradient is also maintained.

The three effects are related to thermal transport, and the coefficients are interrelated. The TEP is relatively easily measured and most of the available results are about this coefficient. Focusing attention, therefore, on TEP, we give below, in brief, the basic theory of TEP which serves as a basis for description of TEP in graphene systems. Also discussed below is the relation of TEP with other transport coefficients.

2.1. Definition and general relations

The thermoelectric effect is due to the interdependence of potential and temperature gradient in a system where no electric current flows. The absolute TEP, S , which is a unique physical property of a material is defined by the relation [29, 30]

$$\mathbf{E} = S \nabla T \quad (10)$$

under open-circuit conditions, where \mathbf{E} is the effective (that is, measured) electric field produced by the temperature gradient ∇T . Since \mathbf{E} and ∇T are vector quantities, S is generally, a tensor.

There are, in general, two contributions to the TEP of the system, namely, the electron-diffusion TEP and the phonon-drag TEP. They will be described later in 2.1.2.

2.1.1. Transport coefficients and thermopower

One can write an expression for the thermoelectric power, S , in terms of the fundamental transport tensors. The equations for the electric current density \mathbf{J} and the heat current density \mathbf{U} , in the presence of a weak electric field and a small temperature gradient, may be written as [8, 9, 11, 12, 29, 30]

$$\begin{aligned} \mathbf{J} &= L_{11} \mathbf{E} + L_{12} \nabla T & (a) \\ \mathbf{U} &= L_{21} \mathbf{E} + L_{22} \nabla T & (b) \end{aligned} \quad (11)$$

where the coefficients, L_{ij} , are, in general, tensors. In order to relate the coefficients to the experimentally measured quantities, such as TEP, it is usual to invert Eq. (11) and write

$$\begin{aligned} \mathbf{E} &= \sigma \mathbf{J} + S \nabla T & (a) \\ \mathbf{U} &= \Pi \mathbf{J} - \kappa \nabla T & (b) \end{aligned} \quad (12)$$

Here

$$\begin{aligned}
 \rho &= (L_{11})^{-1} = \sigma^{-1} & (a) \\
 S &= - (L_{11})^{-1} L_{12} & (b) \\
 \Pi &= (L_{11})^{-1} L_{21} & (c) \\
 \text{and} \\
 \kappa &= L_{21} (L_{11})^{-1} L_{12} - L_{22} & (d)
 \end{aligned}
 \tag{13}$$

are the electrical resistivity, the thermopower, the Peltier and the thermal conductivity tensors, respectively; σ is the electrical conductivity tensor. The coefficients in Eq. (11) are not independent. The Onsager relations say that L_{11} and L_{12} are symmetric and [11]

$$L_{12} = - L_{21}^T / T \tag{14}$$

with the superscript (T) meaning the transpose. The TEP, S , determined under open circuit conditions (that is, with $\mathbf{J} = 0$), is given by Eq. (13b) and can also be expressed as

$$S = (L_{11})^{-1} L_{21} / T = \Pi / T \tag{15}$$

This is known as the second Kelvin relation.

There are two approaches to the evaluation of TEP, S . One can evaluate S directly from the defining relation (10). In this method, usually referred to as the 'Q' approach [9], we need to consider the effect of the electric field and the temperature gradient, simultaneously. One can eliminate the necessity of incorporating a spatially varying temperature in the theory of thermoelectric phenomena by using the Kelvin relation (15), which provides a convenient way of calculating TEP. Instead of a direct calculation of S , we may first determine the Peltier coefficient Π from the solution of an electric conduction problem assuming the temperature gradient to be zero. Imposing the isothermal condition ($\nabla T = 0$), Eq. (11) give

$$\begin{aligned}
 \mathbf{U} &= \Pi \mathbf{J} & (a) \\
 \text{with} & & (16) \\
 \mathbf{J} &= \sigma \mathbf{E}. & (b)
 \end{aligned}$$

S is, then, easily obtained using Kelvin's relation:

$$TS = \sigma^{-1} L_{21} = \Pi = \mathbf{U} / \mathbf{J} = \rho (\mathbf{U} / \mathbf{E}) \tag{17}$$

This method of computing S from Π , advocated by Herring [31] is, usually, known as the Π -approach.

2.1.2. Diffusion and Phonon-drag thermopower

As mentioned earlier, there are two contributions to the thermopower, S , of a system. They are the diffusion TEP and the phonon-drag TEP. In the presence of a temperature gradient the electrons diffuse through the specimen interacting with a random distribution of scattering centres that are assumed to exist in thermal equilibrium at the local temperature T . The heat flux, \mathbf{U}_d , carried by the electrons yields the electron-diffusion thermopower, S_d .

When the assumption of the phonon system being in equilibrium is lifted (which is true, especially, at low temperatures) an additional contribution to S appears — the phonon-drag TEP. The principle of phonon-drag is simple. The phonon flux occurring under the temperature gradient will now less readily dissipate its energy and momentum to the lattice than to the electrons *via* the phonon-electron interaction. There is a net additional momentum imparted to the electrons moving down the temperature gradient. The phonon current thus ‘drags’ electrons with it and extra electrons tend to pile up at the cold end over and above those electrons which are there as a result of the diffusion processes [8, 9, 11, 29, 30]. The heat flux, \mathbf{U}_g , carried by the phonon system yields the phonon-drag TEP, S_g .

The total heat current density \mathbf{U} , therefore, consists of two parts:

$$\mathbf{U} = \mathbf{U}_d + \mathbf{U}_g \quad (18)$$

and, correlatively, the total TEP, S , can be expressed as

$$S = S_d + S_g \quad (19)$$

The treatment presented here is quite general and is applicable to graphene systems.

One can make a simplistic estimate of the magnitude of the diffusion thermopower [11]. It follows from Eq.(16a) that the Peltier coefficient Π , being the ratio of the rate of heat flow to the electrical current, is just the heat per unit charge. For a non-degenerate electron gas, the thermal energy per carrier will be $\sim k_B T$, so that $\Pi \sim \pm k_B T / |e|$ and, from Eq. (15), $S \sim \pm k_B / |e| \sim 86 \mu\text{V/K}$. This suggests that S is a measure of the ratio of the average entropy to the charge. For the degenerate case, the average thermal energy will be reduced by $\sim k_B T / E_F$, so that

$$S \sim \pm (k_B / |e|) (k_B T / E_F) \quad (20)$$

Eq.(20) suggests a linear temperature dependence, usually observed in degenerate systems at higher temperatures when the phonon-drag is unimportant.

2.2. Survey of experimental work

Fundamentally related to the electrical conductivity of a material, the TE transport coefficients are also determined by the band structure and scattering mechanisms operative, and can offer unique information complementary to the electrical transport coefficients. The minimal conductivity at the Dirac point is characteristic of graphene [1-3]. Away from the Dirac point, the electron concentration dependence of conductivity depends on the nature of the scatterers. At low temperatures, the conductivity of graphene is limited by scattering off impurities and disorder which depend on the sample preparation. In the absence of extrinsic scattering sources, phonons constitute an intrinsic source of scattering [3].

Measurements of the thermoelectric properties of graphene have helped elucidate details of the unique electronic structure of the ambipolar nature of graphene, which cannot be probed by conductivity measurements alone. Table 2 lists the recent experimental investigations made with regard to the thermoelectric properties of graphene. Here, we primarily review the measurements made in the absence of an applied magnetic field. The presence of a magnetic field is expected to reveal some more interesting important features, as in conventional 2DEG [11, 16-18, 32].

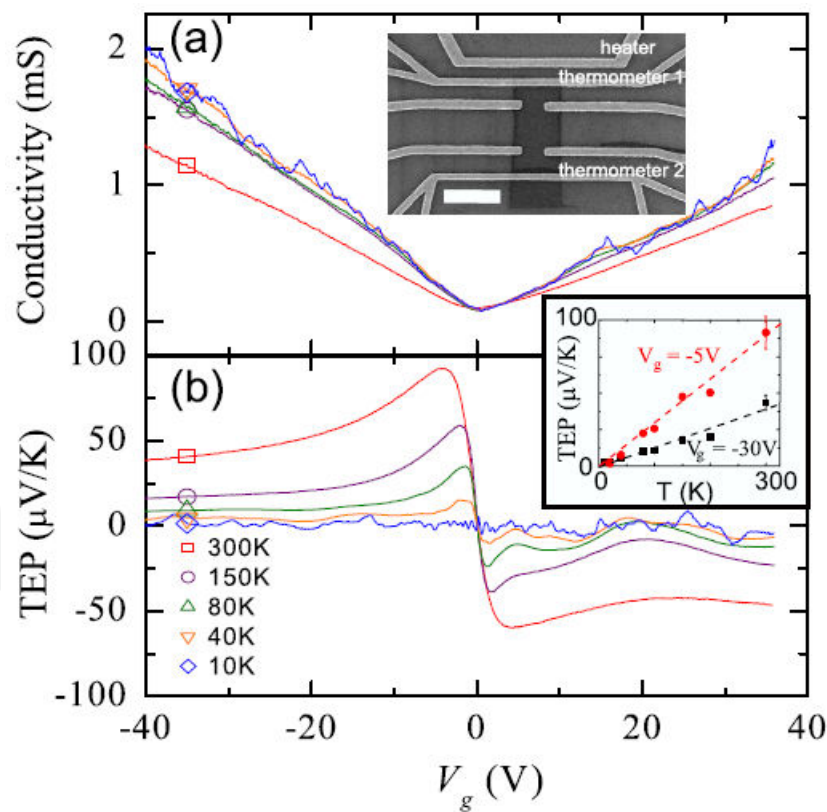


Figure 4. (a) Conductivity and (b) TEP of a graphene sample as function of V_g for $T=300$ K (square), 150 K (circle), 80 K (up triangle), 40 K (down triangle), and 10 K (diamond). Upper inset: SEM image of a typical device, the scale bar is 2 μ m. Lower inset: TEP values taken at $V_g = -30$ V (square) and -5 V (circle). Dashed lines are linear fits to the data. (from [16])

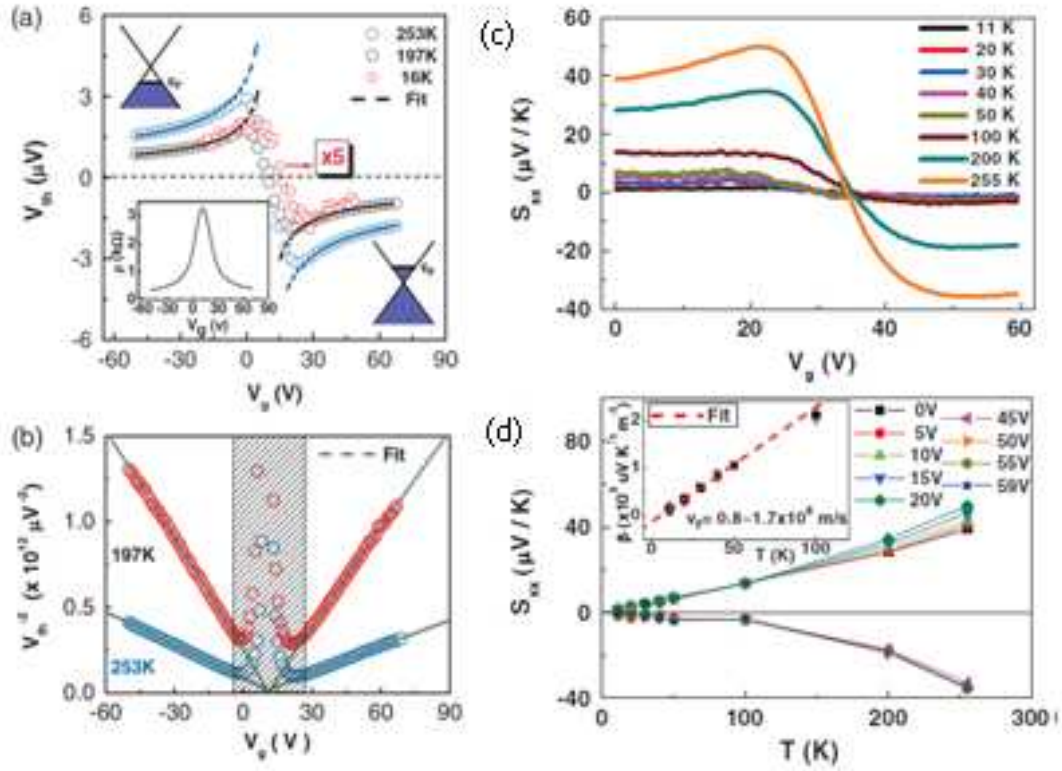


Figure 5. (a) V_{th} vs V_g for three different temperatures. The 16 K data (red circle) were multiplied by a factor of 5. The dashed lines are the fits described by $|S_{xx}| \sim 1/\sqrt{|V_g - V_D|}$. (b) $1/V_{th}^2$ vs V_g plot for the same data shown in (a). The shaded area is for $|V_g - V_D| < 10$ V. Green dashed lines are the best power-law fits with exponent ~ 0.95 . (c) V_g dependence of longitudinal Seebeck coefficient S_{xx} at different temperatures (11–255 K) and zero magnetic field. (d) T dependence of S_{xx} at different gate voltages. The inset is the T dependence of $\beta = S_{xx}\sqrt{|n_{2D}|}$ at $V_g = 0$ V for low temperatures. (from [17])

The TE effect of Dirac electrons has been initially experimentally investigated in graphene samples mechanically exfoliated on ~ 300 nm SiO_2/Si substrates [16–18]. The number of layers in graphene samples can be identified by optical contrast of the samples cross correlated with scanning probe studies and Raman spectroscopy. A controlled temperature difference ΔT is applied to the sample by a heater and the resulting thermally induced voltage ΔV is measured by the voltage probes to acquire the TEP, $S = -\Delta V/\Delta T$. In a typical set up (Figure 1.c) the underlying degenerately doped silicon substrate acts as a gate electrode for modulating the graphene carrier density. The TEP of graphene can be modulated by the gate voltage, V_g . The nonexistence of a gap in the graphene carrier dispersion as in SLG leads to a direct transition between electron-like transport to hole-like transport as the gate voltage is tuned through the charge neutral Dirac point.

Zuev *et al* [16] measured simultaneously the conductance and TEP of different SLG samples. Figure 4 shows the measured electrical conductivity and TEP as a function of applied gate voltage V_g over a temperature range of 10–300 K. The conductivity becomes minimum at the CNP, corresponding to $V_g = V_D$, where the Dirac point $V_D = 0$ V for the device (shown in figure 4). They observe a change in sign of the TEP across the CNP ($V_D = 0$ V) as the majority carrier

density changed from electrons to holes. The linear temperature dependence of TEP shown (inset) for two values of V_g , far away from the CNP suggested that the mechanism for thermoelectric generation is diffusive TEP, with the phonon-drag component not present.

Wei *et al* [17] reported similar experimental results and showed that TE transport is uniquely sensitive to the electronic band structure. Away from the Dirac point, the magnitude of the thermovoltage, V_{th} , decreases, scaling approximately with $|V_g - V_D|^{-1/2}$; the dependence is more noticeable in the linear dependence of V_{th}^{-2} on V_g (see Figure 5.(b)). The divergence of the Seebeck coefficient S_{xx} as $n_s^{-1/2}$, it may be noted, is a direct manifestation of the linear dispersion of Dirac particles in graphene. Because, assuming the energy dependence as $\sigma \sim E^\alpha$, for conductivity of such a highly doped 2D system, the Mott relation [11] yields $S_{xx} \sim -|V_g - V_D|^{-1/2}$. This is in contrast to conventional 2D systems with a quadratic dispersion relation, for which $S_{xx} \sim n_s^{-1}$. Measurements of S_{xx} on a different device with $V_D \sim 33$ V, have indicated (see Figure 5. (c)) electron-hole asymmetry. On the hole side S_{xx} decreases with decreasing V_g , whereas on the electron side S_{xx} remains flat. Further, S_{xx} is found to follow different T dependence for different V_g ; S_{xx} is nearly straight on the hole side, whereas, on the electron side, it remains nonlinear in T except at very low temperatures (see Figure 5.(d)). Wei *et al* attribute the departure from the linear T dependence on the electron side to the asymmetric nature of the band of impurity states, which in the impurity scattering model, can be highly asymmetric near Dirac point [33]. This observation brings out the anomalous TE transport in graphene, which may be used as a sensitive probe for impurity bands near the Dirac point.

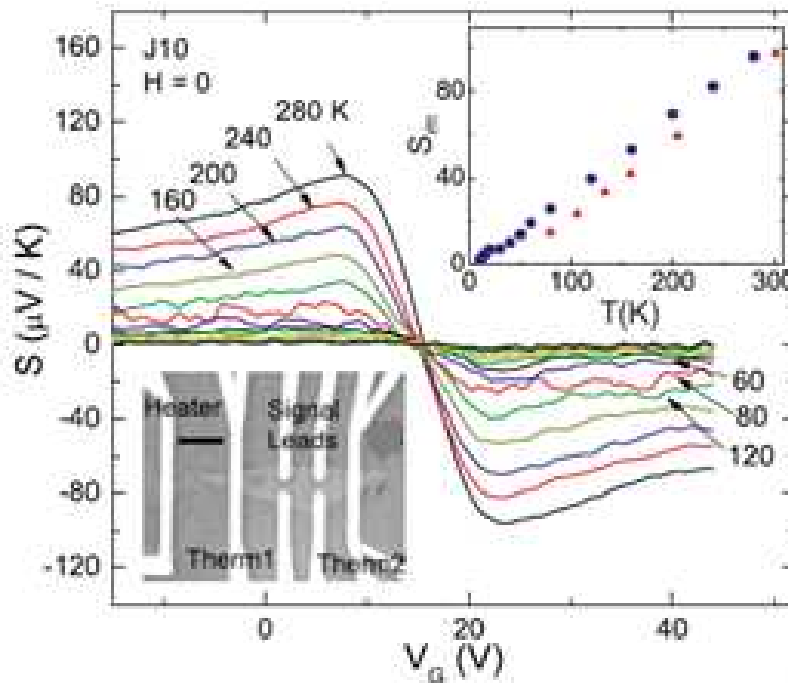


Figure 6. Curves of TEP, $S = -S_{xx}$ vs V_g in sample J10 (left inset) in zero magnetic field at selected T . The curves are anti-symmetric about the Dirac point which occurs at the offset voltage $V_0 = 15.5$ V. The peak value S_m (right inset) is nominally linear in T from 25 to 300 K. (from [18])

Sample	Measurements	Value	Ref.
Single Layer Graphene (SLG)			
Mechanical exfoliation on 300nm SiO ₂ substrate; $\mu \sim 1\text{--}7 \times 10^3 \text{ cm}^2/\text{Vs}$	Gate-dependent conductance and TEP measured simultaneously in zero and non-zero magnetic fields, in linear response regime ($\Delta T \ll T$); T (10-300K); $S_{xx}(B)$ and $S_{xy}(B)$ quantized	$\sim 80 \mu\text{V/K}$ @ RT	[16]
Mechanical exfoliation on 300 nm SiO ₂ substrate; $\mu \sim 3 \times 10^3 \text{ cm}^2/\text{Vs}$	Gate voltage (V_g) and temperature dependent TEP measured in zero & applied magnetic fields; $S(T)$ different for different V_g , S_{xx} diverges near CNP as $n_s^{-1/2}$; Oscillating dependence of both S_{xx} & S_{xy} on n_s @ low T	At $T=255 \text{ K}$, $S_{xx} \sim 39 \mu\text{V/K}$; $S_{xy} \sim 50 \mu\text{V/K}$ @ $B=8 \text{ T}$, @ CNP	[17]
Exfoliation on 300 nm SiO ₂ /Si substrate	V_g dependent TEP in zero and non-zero magnetic fields; $S_m^{\text{peak}}(T)$ is linear S_{xx} & S_{yx} show strong quantum oscillations as functions of V_g .	$\sim 100 \mu\text{V/K}$ @ RT	[18]
Exfoliated & supported on SiO ₂ ; W: 1.5–3.2; L: 9.5–12.5 μm ; G1: 3.2 μm parallel to 1.5 μm G2: 2.4 μm $\mu = 20 \times 10^3 \text{ cm}^2/\text{Vs}$;	Temperature dependence of TEP $S(T)$ curve fitted using theoretical model [35].	G1, G2: $\sim 80 \mu\text{V/K}$ @ RT	[34]
Exfoliated from Kish graphite/ HOPG; $\mu \sim 1.5 - 13 \times 10^3 \text{ cm}^2/\text{Vs}$; $n_i = 3.3 \times 10^{16} \text{ m}^{-2}$	V_g dependence of TEP for $100 < T < 295 \text{ K}$ Effect of charged impurities on the TEP near the Dirac point High μ sample: Mott relation fails near CNP; high T effects obtain agreement Low μ sample: Mott relation holds for all V_g ; charged impurities induce high residual n_s	$\sim 60 \mu\text{V/K}$ @ 295 K	[36]
Epitaxial on C-face of SiC hole-doped: $n_s \sim 10^{12} \text{ cm}^{-2}$; $\mu \sim 20 \times 10^3 \text{ cm}^2/\text{Vs}$ @ 4 K	Temperature dependence of TEP $S_{xx}(T)$ nonlinear: $AT + BT^2$; $S_{xx}(B)$ shows quantum oscillations in $(1/B)$; Sign change observed for S_{yx} , suppression of S_{xx} peak	$\sim 55 \mu\text{V/K}$ @ 230 K	[41]
Exfoliated on SiO ₂ /Si using e-beam lithography; $\mu \sim 4.56 - 12.9 \times 10^3 \text{ cm}^2/\text{Vs}$	V_g dependence of TEP of device for three mobility states S_{xx}^{peak} increases with mobility; Effect of carrier mobility on $S(B)$	$\sim 50 - 75 \mu\text{V/K}$, @ 150 K	[32]
Fabricated on SiO ₂ /Si with e-beam lithography; $\mu \sim 12.9 \times 10^3 \text{ cm}^2/\text{Vs}$	Low- T longitudinal and Hall resistivities (R_{xx} , R_{xy}) and Seebeck and Nernst coefficients (S_{xx} and S_{xy}) in quantizing magnetic fields, B .	$S_{xx}^{\text{peak}} \sim 10 \mu\text{V/K}$ @ 20 K	[39]
Suspended Cu-CVD SLG	The T dependence of TEP for $50 < T < 300 \text{ K}$	$9 \mu\text{V/K}$ @ 300 K	[45]
Few atomic layer thick, cm size sample CVD grown on Si/SiO ₂ /Ni substrates $\rho \sim 3 \times 10^{-5} \Omega\text{cm}$	The T dependence of TEP for $75 < T < 300 \text{ K}$	$10 \mu\text{V/K}$ @ 300 K	[46]
Bilayer Graphene (BLG)			
Mechanical exfoliation on 300 nm SiO ₂ /Si substrate;	S_{xx} as function of V_g and T for $15 < T < 300 \text{ K}$ $S_{yx}(T)$ dependence on disorder	$ S_m \sim 95 \mu\text{V/K}$ @ 300 K	[51]

Sample	Measurements	Value	Ref.
$\mu \sim 2.6 \times 10^3 \text{ cm}^2/\text{Vs}$			
Mechanical exfoliation on 300 nm SiO ₂ /Si substrate; $\mu \sim 2 - 4 \times 10^3 \text{ cm}^2/\text{Vs}$	V_g dependence of TEP measured in BLG for various T $S \propto T$ for large n_s , low T ; Deviation from Mott relation for low n_s @ large T ; Oscillations in $S_{xx}(B)$ and $S_{xy}(B)$ with n_s observed for high B	$\sim 100 \mu\text{V/K}$ @ 250 K	[49]
Mechanical exfoliation on 300 nm SiO ₂ /Si substrate; $\mu \sim 2 - 3 \times 10^3 \text{ cm}^2/\text{Vs}$	Electric field tuning of TEP in Dual-Gated BLG demonstrated – originates from band-gap opening; Enhanced TEP;	$S_m^{\text{peak}} \sim 180 \mu\text{V/K}$ @ 250 K	[52]
Single Layer-Multi Layer Graphene (SLG-MLG)			
S-BLG transistor; Mechanical exfoliation of graphene sheets onto 90 nm SiO ₂ /Si wafer; SLG/BLG identified by optical contrast & Raman	Optoelectronic response of S-BLG interface junction using photocurrent microscopy as function of V_g (Photocurrent is by photo-TE effect)	$\sim 6 \mu\text{V/K}$ @ 12 K	[53]
SLG - TLG epitaxial on 6H-SiC	TEP (over 300 – 550 K) as function of environment composition	p: $10 \mu\text{V/K}$ n: $-20 \mu\text{V/K}$ (annealed @ 500K)	[54]
SLG-MLG CVD on Cu	Layer-dependence of the graphene Seebeck coefficient is peculiar & unexpected, that exceptionally increases with increasing thickness Gas flow induced voltage in MLG is not proportional to S	$\sim 30 \mu\text{V/K}$ (SLG) $- 54 \mu\text{V/K}$ (HLG) @ RT	[55]
Few Layer Graphene (FLG)			
FLG Pristine: on SiO ₂ /Si substrate, $t \sim 5\text{nm}$ with possible structural defects; Treated: ACN, TPA attachments	Temperature dependence of TEP Power Factor Enhancement for Few-Layered Graphene Films by Molecular Attachments TEP increased ~ 4.5 times Results supported by simulations based on Kubo's formula	Pristine: $\sim 40 \mu\text{V/K}$ Treated: $180 \mu\text{V/K}$; $300 < T < 575 \text{ K}$	[56]
FLG On SiO ₂ /Si substrate; SLG & rGO	Temperature dependence of TEP Enhanced TEP of films with Oxygen Plasma Treatment Treatment generates disorders which open the π - π^* gap leading to enhancement of TEP and reduction in σ	FLG: Pristine: $\sim 80 \mu\text{V/K}$ Treated: $\sim 700 \mu\text{V/K}$ @ 575 K; SLG: p @ low T & n @ high T ; $S \sim -40$ to $50 \mu\text{V/K}$	[57]

Table 2. Measurements of thermopower in graphene

Checkelsky and Ong [18] have also reported measurements of TEP, S , and Nernst, S_{yx} , signals in graphene in non-zero and zero magnetic fields. In the absence of a magnetic field, they observe, besides the change in sign of S with V_g , a nominally linear-in- T dependence of the peak value S_m from $\sim 20 \text{ K}$ to 300 K (see Figure 6).

Seol *et al* [34], in their study of the thermal properties of graphene, have reported measurements of electrical conductivity, TEP and thermal conductivity of SLG flakes. They obtain room-temperature values of $\sim -80 \mu\text{V/K}$ for the Seebeck coefficient (S). They fit their data on the temperature dependence of S using the semiclassical theoretical model of Hwang *et al* [35], which assumes screened charged impurity scattering to dominate the electron transport. The temperature-dependent screening is found to produce a T dependence of S not captured in Mott formula.

With a view to investigate the effect of charged impurities on the TEP of graphene near the Dirac point, Wang and Shi [36] have measured both TEP and electrical conductivity of SLG samples with varying degree of disorders as characterized by carrier mobilities ranging from $1.5 - 13.0 \times 10^3 \text{ cm}^2/\text{Vs}$, and examined the validity of the Mott relation as the low-density region near the Dirac point is approached. The four-point geometry they employed allowed them to measure the graphene resistivity properly by excluding the contact resistance and ensuring that both σ and V_{th} come from the same locations where the local temperatures are measured. They find that at higher temperatures, the Mott relation holds for low-mobility samples but fails in the vicinity of the Dirac point in high-mobility samples; however, below 100 K the deviation is insignificant even in the highest mobility sample. The reason for such a behaviour could be that, in the case of high-mobility graphene, the carrier density near the CNP can be so low that $k_B T \ll E_F$ no longer holds. It may be noted that the Mott relation is only an approximation for degenerate electron systems when T is far below the Fermi temperature. In low-mobility samples, on the other hand, the charged impurities are many and could induce relatively high residual carrier density near CNP so that $T_F \gg T$ and the Mott relation holds at all gate voltages. Wang and Shi suggest that, by properly taking account of the high-temperature effects, the Boltzmann transport theory can satisfactorily explain the experimental data on Seebeck coefficient in low-density electron systems near CNP.

In their recent measurements, shown in Figure (7), Shi and co-workers [32] have investigated the carrier mobility-dependence of TE transport properties of SLG in zero and non-zero magnetic fields. In the absence of magnetic field, they find that, with increase in mobility, the maximum value of S_{xx} increases, and exhibits an increasingly diverging trend accompanied by a sharper peak-to-dip transition around Dirac point. They find that the peak-to-dip width is related to the width of the minimum conductivity plateau, which is broader for the low-mobility state, and is known to be associated with disorder in graphene. Further, S_{xx} is found to converge to the same values at high gate voltages on either side of CNP, for all mobility values. This suggests that the effective carrier density is much greater than the charge density fluctuations induced by charged impurities near the Dirac point.

The magnetic field dependence of TEP has also been studied [16-18, 32]. In a magnetic field, carriers diffusing under the temperature gradient experience a Lorentz force, resulting in a non-zero transverse voltage. In the quantum Hall regime at a high magnetic field, the curves of S vs V_g show pronounced oscillations reflecting Landau quantization of the Dirac states. The peaks in S are aligned with those in conductance. The TEP and Nernst signals, which show quantized behaviour, are in agreement with the generalized Mott relation, except for strong deviations near the CNP. A Nernst signal, $S_{xy} \sim 50 \mu\text{V/K}$ at 8 T is observed near the Dirac point

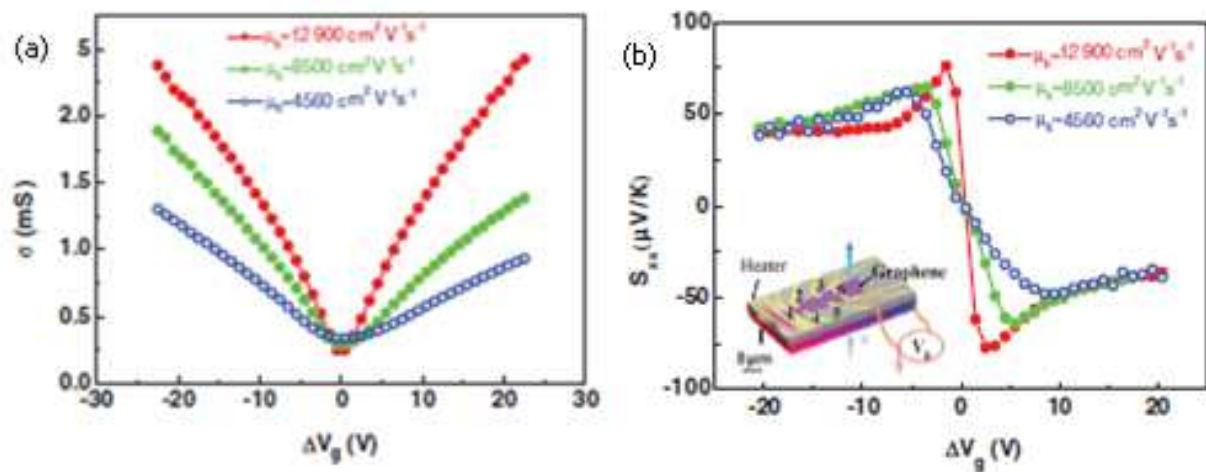


Figure 7. Gate voltage dependence of (a) Electrical conductivity, σ , and (b) Seebeck coefficient, S_{xx} , of device A at 150 K with three hole mobility values 12900, 8500 and 4560 $\text{cm}^2 \text{V}^{-1} \text{s}^{-1}$. Inset of (b) shows SEM image of the device. (from [32])

($n = 0$ LL). Such an enhancement of the Nernst signal is predicted in conventional 2D electron systems, and depends on the disorder strength [37, 38]. However, the observed large Nernst peak and the strong suppression of S at $n=0$ LL are inconsistent with the flat-top profiles calculated for a 2D system with quadratic dispersion. Shi and co-workers [32, 39] have investigated the dependence of the magneto-TE transport properties of graphene on electrical transport. They find, by independently varying the magnetic field and carrier density, that the derivative relation between S_{xx} and S_{xy} , discovered in conventional 2DEG systems, holds for graphene for high LLs except near the Dirac point, where different mechanisms such as carrier localization may be responsible.

Samples grown by different methods throw light on the different characteristics of TEP in graphene systems. The main graphene production techniques include dry and wet exfoliation, photo-exfoliation, growth on SiC, CVD, MBE and chemical synthesis (for a recent review see [40]). Although initially graphene samples have been mechanically exfoliated, with a view to investigate the TE characteristics further, the samples have been produced by other methods as well.

Wu *et al* [41] have investigated the TE response of relatively high-mobility ($\sim 20 \times 10^3 \text{ cm}^2/\text{Vs}$ at 4 K) SLG grown epitaxially on SiC substrates. For a carrier (hole) density of $1 \times 10^{12} \text{ cm}^{-2}$, away from the Dirac point, the temperature dependence of TEP displays a deviation from the Mott relation. The data is found to obtain a least square fit to $AT+BT^2$, where A and B are temperature independent constants. The additional quadratic dependence instead of the otherwise linear dependence reflects the importance of the screening effect. The dielectric constant of SiC being a factor of 2 higher than that of SiO_2 , the effect of screening is expected to be stronger in epitaxial graphene. Hwang *et al* [35] have shown that when the screening effect and its temperature dependence are taken into account, a quadratic correction to the TEP appears. In high magnetic fields, in the quantum Hall regime, a suppression of S_{xx} is observed

even for the high mobility sample used. A study [42] finds TEP to be universal in the presence of disorder. The role of disorder needs to be investigated further.

Kim and co-workers [43] report measurement of TEP on graphene samples deposited on hexaboron nitride substrates where drastic suppression of disorder is achieved. Their results show that at high temperatures where the inelastic scattering rate due to electron-electron (e-e) interactions is higher than the elastic scattering rate by disorders, the measured TEP exhibits an enhancement compared to the expected TEP from the Mott relation.

Graphene structures grown epitaxially on metal surfaces could reach sizes up to a micrometer with few defects. They can also be formed on the surface of SiC with the quality and number of layers in the samples depending on the SiC face used for their growth.

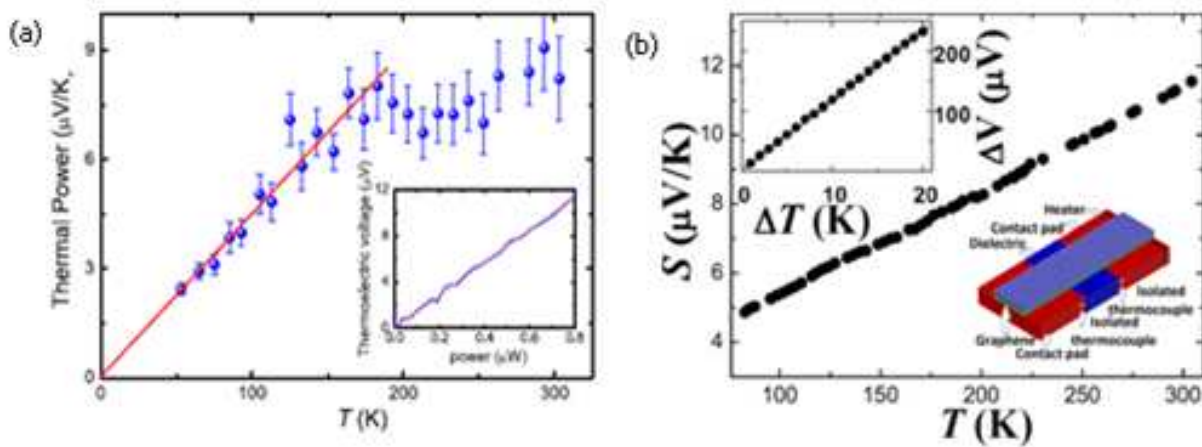


Figure 8. Temperature dependence of TEP measured in CVD-graphene samples of (a) Xu *et al.* [45], and (b) Babichev *et al.* [46]. Insets: (a) TE voltage as a function of applied Joule heat. (b) Upper-left: dependence of the TEP voltage on the applied temperature difference. Lower-right: a schematic view of device used in TEP measurements. (from [45, 46])

The carbon-terminated surface can produce few layers with low mobility whereas the silicon-terminated surface can give many layers with higher mobility [40]. Chemically exfoliating graphene is another method of preparing good quality and large amount of few-layer graphene sheets [44].

There exist a few reports of measurements of TEP of CVD-grown graphene [45, 46]. Figure 8 shows the observed temperature dependences. Other investigations have demonstrated the TEP of CVD-grown graphene to be a sensitive probe to the surface charge doping from the environment and the device concept promises use in gas/chemical sensing [47]. An initially degassed n-type graphene sample, upon exposure to gases, was found to become p-doped or

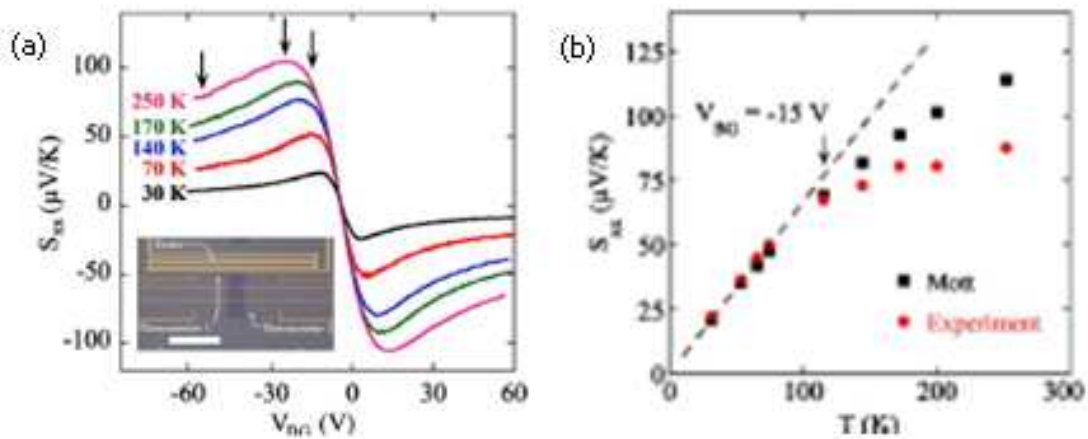


Figure 9. TEP as a function of (a) backgate voltage V_{BG} for $T=30, 50, 70, 140, 170$ and 250 K, and (b) temperature T for $V_{BG}=-15$ V. Inset in (a): optical image of a typical device. (from [49])

further n-doped during exposure depending on the properties of the ambient gases as evidenced by a monotonic change in sign of TEP.

In a graphene sample, the substrate on which the graphene layer is exfoliated, affects the morphology of the graphene specimen and is a source of impurities. In a suspended graphene (SG) sample, on the other hand, the substrate is etched away so that the graphene is suspended over a trench approximately 100 nm deep, with most of the impurities sticking to the graphene sheet [48]. Annealed SG samples showed both ballistic and diffusive carrier transport properties with carrier mobilities more than $2 \times 10^4 \text{ cm}^2/\text{Vs}$. The warping of the layers can be avoided with the use of a top gate [21].

In the case of BLG, Nam *et al* [49] have measured the TEP, S_{xx} , for $30 < T < 250$ K and for different charge-carrier densities. As in SLG, [16-18] the ambipolar nature of the carriers manifests itself as the sign change in Figure 9.(a) at the CNP. Their low- T result of TEP is found to follow the semi-classical Mott formula, and for high carrier densities TEP shows a linear-in- T dependence implying a weak electron-phonon interaction and negligible phonon-drag effect in BLG. For a low carrier density, a deviation from the Mott relation along with a saturating tendency of TEP, is observed at higher temperatures (See Figure 9.(b)) and is attributed to the low Fermi temperature in the BLG.

There do not seem to be till date any reports on measurements of TEP of graphene nanoribbons.

In the following sections, we discuss, based on the Boltzmann formalism, the present theoretical understanding of the observed phenomena, in terms of the diffusion and phonon-drag contributions. An analysis of measured TEP is usually done by separating the two contributions by making use of their characteristic temperature dependences at lower temperatures [11]. Often, in literature, the diffusion component, S_d , for a degenerate system, is assumed to vary linearly with temperature. It may be seen from Eq. (36) that the Mott relation suggests such linear temperature dependence, provided the energy dependence of relaxation time does not vary with temperature, though its magnitude will. S_d , thus, reflects the energy dependence

of a scattering mechanism and is determined not only by the magnitude of scattering, but also by details concerning the distribution of the scatterers and their type. The phonon-drag component, S_g , on the other hand, unlike S_d , depends only on the electron-acoustic phonon coupling strength. Its low-temperature dependence is expected, as in conventional 2D systems, to display a characteristic peak, which exhibits the role of phonon scattering mechanisms. Since the effect of electron-phonon coupling in determining the resistivity of graphene is observed to be weak [50], especially at low temperatures, the phonon drag component has often been assumed to be absent, and an analysis of TEP, for the range of temperatures ($10 < T < 300$ K) investigated in the experiments on graphene, is given based on the diffusion component.

3. Diffusion thermopower

Diffusion thermopower, S_d , is known to provide unique information complementary to the electrical transport coefficients in metals and semiconductors [8-12]. The TE transport coefficients, defined above and related to electrical transport, are determined by the band structure and scattering mechanisms operative in a system. S_d can, therefore, be a sensitive and powerful tool to probe and elucidate details of the thermoelectric transport and understand the carrier transport mechanisms of graphene that cannot be probed by electrical conductivity alone.

In this review, we adopt the Boltzmann approach, found to be robust especially for transport in graphene far away from the Dirac point [58]. We give here, in brief, the basic theory of TEP and the expressions used in the present analysis of S_d in graphene systems.

3.1. Basic formalism – Boltzmann approach

Low field transport in many of the systems is often described by the Boltzmann transport equation (BTE) [59-61]. This semi-classical Boltzmann approach is known to be appropriate for structures in which the potentials vary slowly on both the spatial scale of the electron thermal wavelength and the temporal scale of the scattering processes. The conventional theory of charge carrier transport in 2D semiconductors is based on this formalism, and the TE coefficients are commonly obtained by solving the BTE in the relaxation time approximation [11].

In the regime of large chemical potential, the nature of transport of the massless Dirac fermions through a 2D graphene membrane may be accessed by the Boltzmann formalism [3] and one may write an expression for TEP in graphene systems in terms of the fundamental transport coefficients.

3.1.1. Transport coefficients in graphene systems

We consider a graphene system of length L , and width W to be a 2D homogeneous system of charge carriers, with a density n_s induced by an external gate bias V_g . In the presence of a temperature gradient ∇T applied along the plane of the graphene layer(s), Eq. (12), for the

effective electric field, \mathbf{E} , and the heat current density, \mathbf{U} , under open circuit conditions ($\mathbf{J} = 0$), reduce to

$$\mathbf{E} = S \nabla T \quad (21)$$

and

$$\mathbf{U} = \kappa (-\nabla T) \quad (22)$$

The electric current density, and heat current density, can be evaluated by solving the Boltzmann transport equation in the relaxation time approximation. Assuming the electric field to be weak and the displacement of the distribution function from thermal equilibrium to be small, the electron distribution function $f(E_k)$ can be written as [29, 30]

$$f(E_k) = f^0(E_k) + \tau(E_k) \mathbf{v}_k \cdot \left[e\mathbf{E} - \left(\frac{E_k - E_F}{T} \right) \nabla T \right] \left(-\frac{\partial f^0(E_k)}{\partial E_k} \right) \quad (23)$$

where, \mathbf{v}_k is the velocity of the electrons in state \mathbf{k} , $\tau(E_k)$ is the electron momentum relaxation time, $f^0(E_k)$ is the equilibrium Fermi-Dirac distribution function and E_F is the Fermi energy which is determined by the carrier density

$$n_s = \int \rho(E_k) f^0(E_k) dE_k \quad (24)$$

with $\rho(E_k)$ denoting the density of states of the system.

In Eqs. (11a) and (11b), the current densities \mathbf{J} and \mathbf{U} , can be evaluated from the expressions:

$$\mathbf{J} = (g_s g_v / At) \sum_k e \mathbf{v}_k f(E_k) \quad (25)$$

and

$$\mathbf{U} = (g_s g_v / At) \sum_k (E_k - E_F) \mathbf{v}_k f(E_k) \quad (26)$$

Here, g_v and g_s denote the valley and spin degeneracies, $A=LW$ is the area of the surface and ' t ' the layer thickness of the graphene system. Using Eqs.(21) – (23), \mathbf{J} and \mathbf{U} can be expressed as [29]

$$\mathbf{J} = e^2 K_{11} \mathbf{E} + (e/T) K_{12} (-\nabla T) \quad (27)$$

$$\mathbf{U} = e K_{21} \mathbf{E} + (1/T) K_{32} (-\nabla T) \quad (28)$$

where the coefficients K_{rs} are given by

$$SLG \quad K_{rs} = \frac{1}{t\pi\hbar^2} \int_0^\infty E_k (E_k - E_F)^{r-1} \tau^s(E_k) \left(-\frac{\partial f^0(E_k)}{\partial E_k} \right) dE_k \quad (a)$$

$$BLG \quad K_{rs} = \frac{m^*}{2t\pi\hbar^2} \int_0^\infty v_k^2 (E_k - E_F)^{r-1} \tau^s(E_k) \left(-\frac{\partial f^0(E_k)}{\partial E_k} \right) dE_k \quad (b) \quad (29)$$

$$AGNR \quad K_{rs} = \frac{2}{Wt\pi\hbar} \sum_n \int_{E_n}^\infty v_k (E_{n,k_y} - E_F)^{r-1} \tau^s(E_{n,k_y}) \left(-\frac{\partial f^0(E_{n,k_y})}{\partial E_{n,k_y}} \right) dE_{n,k_y} \quad (c)$$

In the absence of temperature gradient ($\nabla T = 0$), Eq. (27) gives electrical conductivity as

$$\sigma = e^2 K_{11} \quad (30)$$

From Eqs. (21), (22), (27) and (28), one obtains expressions for the diffusion contribution to thermopower, S_d , and for electronic thermal conductivity, κ_e as

$$S_d = \frac{1}{eT} K_{11}^{-1} K_{21} \quad (31)$$

and

$$\kappa_e = \frac{1}{T} \left[K_{31} - \left(K_{31} \right)^2 / K_{11} \right], \quad (32)$$

respectively. Equation (31) may be expressed as [11]

$$S_d = \frac{1}{eT} \left(\frac{\langle E_k \tau(E_k) \rangle}{\langle \tau(E_k) \rangle} - E_F \right) \quad (33)$$

$$\text{with } \langle F(E_k) \rangle = \frac{\int F(E_k) E_k (-\partial f^0 / \partial E_k) dE_k}{\int E_k (-\partial f^0 / \partial E_k) dE_k}$$

Equations (30) – (33) show that evaluation of the transport coefficients requires a knowledge of the relaxation time(s), $\tau(E_k)$. Note that the overall contribution to S_d and κ_e , from the various scattering mechanisms operative in the system, can be evaluated assuming the overall relaxation time $\tau(E_k)$ to be given by Matthiessen's rule [11, 29, 30]:

$$\tau^{-1}(E_k) = \sum_j \tau_j^{-1}(E_k), \quad (34)$$

where the sum is over all the relevant scattering mechanisms, j .

Often in literature, limiting forms of S_d are used in the analysis of data. In the degenerate limit a good approximation to Eq. (32) is the well-known Mott expression [11, 29, 30]:

$$S_d = \frac{\pi^2 k_B^2 T}{3e} \left[\frac{d \ln \sigma(E_k)}{dE_k} \right]_{E_k=E_F}, \quad (35)$$

where, $\sigma(E_k)$, is the energy dependent conductivity. If the energy dependence of relaxation time is taken as $\tau(E) \sim E^p$, Eq. (35) can be more simply expressed for the three graphene systems, as [35, 62-65]

$$\begin{aligned} \text{SLG, BLG} \quad S_d &= \frac{\pi^2 k_B^2 T}{3e E_F} [p + 1] & (a) \\ \text{AGNR} \quad S_d &= \frac{\pi^2 k_B^2 T}{3e E_F} \left[p + \left(\left(\frac{E_F}{E_n} \right)^2 - 1 \right)^{-1} \right] & (b) \end{aligned} \quad (36)$$

where the first term reflects the scattering mechanisms. The parameter p can also be expressed in the form

$$p = \frac{E_F}{\tau(E_F)} \left[\frac{d\tau(E_k)}{dE_k} \right]_{E_k=E_F}. \quad (37)$$

Eq. (37) brings out the feature that S_d is determined by not only the magnitude of scattering but also by the energy dependence of $\tau(E_k)$ at $E_k = E_F$. It may be noted that provided the energy

dependence of $\tau(E_k)$ does not vary with temperature (though its magnitude will), S_d will be a linear function of temperature.

A solution of the Boltzmann equation in the relaxation time approximation may be applied exactly when the important collision processes are all elastic [30, 59-61]. It is also applicable when the inelastic processes include non-polar optic and intervalley phonon scattering. If polar optic phonon scattering is also important, the method is applicable only at high temperatures. Solutions of Boltzmann equation when polar optic phonon scattering is dominant may be obtained by applying variational or numerical methods.

3.2. Scattering mechanisms

Central to understanding the TE transport properties of graphene, are the mechanisms causing the scattering of the charge carriers. A better understanding, therefore, of the relative importance of the operative scattering mechanisms, which varies with temperature and carrier concentrations in graphene, enables useful improvements in the transport properties of graphene for various possible TE applications.

Scattering in graphene which could contribute to carrier transport may result from both intrinsic and extrinsic sources. The extrinsic sources may be vacancies, surface roughness arising from rippling of the graphene sheet, disorder, which can create electron-hole puddles, and charged impurities, known to be the main scattering mechanism in graphene. Apart from the graphene layers, the substrates may also be a source of impurities. Besides, there are additional scattering sources such as neutral point defects [1, 3]. In principle, the limitation due to the extrinsic scattering mechanisms can be reduced by improved growth/fabrication techniques.

In the absence of extrinsic scattering sources, phonons, which constitute an intrinsic source of scattering in a system, limit carrier mobility at finite temperatures [59-61]. Phonon scattering may be due to intravalley acoustic and optical phonons which induce the electronic transitions within a single valley, and intervalley phonon scattering that induces electronic transitions between different valleys [3]. The intravalley acoustic phonon scattering, induced by low energy phonons and considered an elastic process, gives a quantitatively small contribution in graphene even at room temperature due to the high Fermi temperature of graphene. Shishir *et al* [66] in their calculations of mobility and resistivity, respectively, including contributions of optical phonon scattering, found that the effect of optical phonons cannot be neglected. The role of remote interface polar optical phonons in the substrate in graphene transport also seems to be important.

In the case of SG, the intrinsic scattering mechanisms limiting electron transport in SG layers are due to in-plane and out-of-plane (flexural) acoustic phonons. Recent investigations of electron and phonon transport in SG indicate that in the free standing case (absence of strain) the major contribution to resistivity and thermal conductance is from acoustic flexural phonons, and this intrinsic limitation can be reduced by the effect of strain [28, 67].

Evaluation of the transport coefficients requires the knowledge of the relaxation times of the scattering mechanisms. In the following, we give the expressions for the momentum relaxation times of the extrinsic and intrinsic scattering mechanisms.

3.2.1. Relaxation times

The expressions for the momentum relaxation times for the various scatterings in graphene systems may be expressed as [3]

$$\frac{1}{\tau_j(E_k)} = \frac{2\pi}{\hbar} \sum_{k'} \sum_q |C_j(q)|^2 F(\theta) (1 - \cos(\theta)) \Delta(E_k, E_{k'}) \quad (38)$$

where ' θ ' is the angle between initial (k) and final states (k'), and $|C_j(q)|^2$ is the matrix element for the interaction of electrons with the scattering source, ' j '. The form factor, $F(\theta)$, due to the overlap of the wavefunctions and arising due to the chiral nature of the graphene carriers, is

$$\text{given by [3, 27]} \quad F(\theta) = \frac{1}{2}(1 + \cos(\theta)) \text{SLG}, \quad F(\theta) = \frac{1}{2}(1 + \cos(2\theta)) \text{BLG},$$

$$F(\theta) = \frac{1}{2}(1 + \cos(\theta_{n,k_y} - \theta_{n',k'_y})) \text{AGNR}$$

The overall momentum relaxation time $\tau(E_k)$ can be taken to be given by Matthiessen's rule (Eq.(34)). The factor $\Delta(E_k, E_{k'})$ in Eq. (38) is given, for elastic scatterings, by

$$\Delta(E_k, E_{k'}) = \delta(E_k - E_{k'}) \quad (a)$$

In the case of phonons,

$$\Delta(E_k, E_{k'}) = \frac{N_q [1 - f^0(E_k + \hbar\omega_q)] \delta(E_k - E_{k'} + \hbar\omega_q) + (N_q + 1) [1 - f^0(E_k - \hbar\omega_q)] \delta(E_k - E_{k'} - \hbar\omega_q) \theta(E - \hbar\omega_q)}{[1 - f^0(E_k)]} \quad (b) \quad (39)$$

$$\Delta(E_k, E_{k'}) = \frac{2k_B T}{\hbar\omega_q} \quad (c)$$

In eq.(39b), $\theta(x)$ is the unit-step function and the first (second) term corresponds to the absorption (emission) of a phonon of wavevector \mathbf{q} and energy $\hbar\omega_q$. The phonon distribution N_q is, for low fields, given by the equilibrium Bose distribution, $N_q^0 = (\exp(\hbar\omega_q/k_B T) - 1)^{-1}$. At high temperatures, in the equipartition (EP) regime, where $\hbar\omega_q \ll k_B T$, one may consider scattering of electrons from acoustic phonons to be quasi-elastic and with $N_q \sim k_B T / \hbar\omega_q$, the factor $\Delta(E, E')$ in Eq.(38) becomes (39c). Often, in literature, expressions for electron-acoustic phonon relaxation times obtained in the EP approximation are used in the analysis of transport properties [3].

In the 2D material of graphene at low temperatures, an understanding of electron-phonon interaction is important both from basic physics and technology points of view [3]. In typical conductors, electrons are scattered by phonons producing a finite temperature-dependent resistivity $\rho(T)$ [59-61]. Recent investigations [68] of resistivity of graphene show that there is

a change in temperature dependence of resistivity from $\rho(T) \sim T$, in the high temperature limit, to $\rho(T) \sim T^4$, at low temperatures, reflecting the 2D nature of the electrons and the acoustic phonons in graphene. At low enough temperatures, recent theoretical studies [69] of the phonon-induced graphene resistivity have shown that, the resistivity eventually goes as $\rho(T) \sim T^6$, for screened phonon scattering. At such low temperatures the major contribution to this resistivity is from in-plane acoustic phonons [50, 70]. The crossover between the two distinct regimes can be described by the characteristic Bloch-Gruneisen (BG) temperature defined as $T_{BG} = 2\hbar v_s k_F / k_B$, where v_s is the velocity of sound and $k_F = (\pi n_s)^{1/2}$ is the Fermi wavevector [68]. The electrostatic tunability of the chemical potential, $E_F = \hbar v_F k_F$, in graphene allows for a wide range of control of T_{BG} ; for graphene with $n_s = 1 \times 10^{15} \text{ m}^{-2}$, $T_{BG} \sim 17 \text{ K}$ for LA modes.

The expressions for the momentum relaxation rates for in-plane and flexural acoustic phonon, non-polar optical phonon, surface polar optical phonon and for roughness, impurity and vacancy scatterings in the graphene systems are given in Table 3.

Suspended graphene (SG) allows for the investigation of the intrinsic properties of the material, unperturbed by the presence of a substrate. It has been realized that mechanical deformations of graphene sheets affect the electronic properties. This is of special relevance for strain-engineering aimed at controlling the electronic properties of graphene by suitably engineering the deformations ([67] and references therein). Employing the semi-classical Boltzmann transport formalism, Mariani and Oppen [67] and Ochoa *et al* [28], have studied electron-phonon contribution to resistivity in free-standing SLG and BLG and discussed the role of strain in SG. Restricting to the regime of $T \gg T_{BG}$, and assuming the phonons to couple to electrons through a screened scalar deformation potential (constant g) and a vector potential (β) associated with the changes in bond length between carbon atoms, they have given expressions for the momentum relaxation rates in SG for both free-standing and strained layer cases (see Table 3).

3.3. Diffusion thermopower in graphene systems

Besides the experimental investigations (see Table 1.), the TEP of graphene has also attracted much theoretical attention. The theoretical investigations made to understand the experimental results have so far been mostly on the basis of the diffusion TEP, ignoring the drag component.

The following features of TEP, first observed in SLG samples by Zuev *et al* [16], Wei *et al* [17] and Chekelsky and Ong [18], are found to be characteristic of graphene. The measured TEP reaches a value $\sim 100 \text{ } \mu\text{V/K}$ at room temperature. The sign of TEP changes across the charge neutrality point (CNP) as the majority carriers change from electrons to holes. Away from the CNP, the TEP shows a $n_s^{-1/2}$ dependence on the carrier density n_s . At low temperatures, it exhibits a linear temperature dependence, in consonance with the Mott formula Eq.(36). For higher temperatures, a deviation from Mott formula is observed. Measurements on high mobility graphene samples [51], show that Mott relation fails near the Dirac point. In the case of FLG samples, Li *et al* [55] find that TEP depends on the number of layers, increasing with increase in thickness and reaching a peak value for six layers.

In the presence of a quantizing magnetic field, the TEP of graphene exhibits additional interesting effects [16-18, 32]; however, these do not form the content of the present review. The theoretical studies of S_d of graphene systems, in the absence of magnetic fields, based on the semi-classical Boltzmann formalism are briefed below; the drag component is discussed in the next section.

3.3.1. Diffusion thermopower in SLG

Much of the theoretical investigations of diffusion TEP in graphene has been made on SLG with interest being devoted mostly to the TEP at higher temperatures ($10 < T < 300\text{K}$).

Using a phenomenological theory for transport in graphene, close to Dirac point, based on the semiclassical Boltzmann approach Peres and coworkers [72, 76] have obtained an expression for diffusion TEP including the scattering mechanism involving midgap states arising from local point defects in the form of vacancies, cracks, boundaries, impurities in the substrate or in corrugated graphene. They find that this mechanism leads to a similar k dependence as charged impurities, and show that the dependence of S_d on the particle density is different from that of the conventional 2DEG and of graphene sheet with only charged impurities in the substrate.

Lofwander and Fogelstrom [33], have presented calculations for the linear response to electrical and thermal forces in graphene for the case of strong impurity scattering in the self-consistent t-matrix approximation. At low temperatures, the electronic contribution to TEP is found to be linear in T with slope proportional to the inverse of the impurity density and the impurity strength, so that TEP could provide information about impurities in graphene. Further, for moderately large impurity strengths, a non-linear temperature dependence is obtained and $S \sim 100 \mu\text{V/K}$.

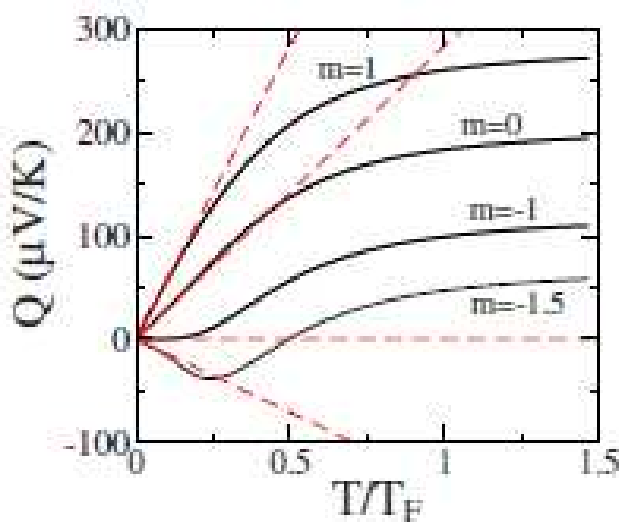


Figure 10. Hole TEP for different energy dependent scattering times, $\tau \sim E^m$. Dashed lines show corresponding Mott variations.(from [35])

Scattering Mechanism	Relaxation Rate, $\tau^{-1}(E)$	Ref.
Single Layer Graphene (SLG)		
Acoustic Phonons	$\frac{2\pi}{\hbar} \int_0^{2\pi\infty} \frac{D_{ac}^2 \hbar q}{2A\rho v_s} \left(1 - \left(\frac{q}{2k}\right)^2\right) \Delta(E_k, E_{k'}) k' dk' d\theta$	[71]
Optical Phonons	$\frac{D_{op}^2}{\rho \omega_{LO} (\hbar v_F)^2} [(E - \hbar \omega_{LO}) (N_q + 1) \theta(E - \hbar \omega_{LO}) + (E + \hbar \omega_{LO}) N_q]$	[66]
Impurities	$\frac{\sqrt{n_i} Z e^2}{\hbar^2 v_F k (4\epsilon \epsilon_0 (1 + (y_i/k_F)))}$	[72]
Surface roughness	$\frac{2k}{v_F} \left(\frac{\Lambda n_s e^2 \Delta}{8\pi \hbar \epsilon \epsilon_0}\right)^2 \frac{1}{\sqrt{1 + k^2 \Lambda^2}} \exp\left(\frac{k \Lambda}{\sqrt{1 + k^2 \Lambda^2}}\right)$	[66]
Vacancies	$\frac{\pi^2 v_F n_{vac}}{k (\ln(k R_0))^2}$	[72]
Suspended Single Layer Graphene (SG) *		
Acoustic Phonons (In-plane)	$\left[\frac{g^2}{2} + \frac{\hbar^2 v_F^2 \beta^2}{4a^2} \left(\frac{1}{v_L^2} + \frac{1}{v_T^2}\right)\right] \frac{E}{2\rho \hbar^3 v_F^2} k_B T$	[28]
Acoustic Phonons (Flexural)	$\left(\frac{g^2}{2} + \frac{\hbar^2 v_F^2 \beta^2}{4a^2}\right) \left[\frac{(k_B T)^2}{64\pi \hbar \kappa^2 E} + \frac{k_B T E}{32\pi \hbar^2 v_F^2 \kappa \sqrt{\rho \kappa}}\right] \ln\left(\frac{k_B T}{\hbar \omega_c}\right)$	[28]
Acoustic Phonons (Flexural) (strained)	$\left[\frac{g^2}{2} + \frac{\hbar^2 v_F^2 \beta^2}{4a^2}\right] \frac{E (k_B T)^4}{16\pi \rho^2 \hbar^5 v_F^2 v_L^6 \bar{u}^3} \times \left[\Re_2\left(\frac{a k_B T}{\hbar v_L^2 \bar{u}}\right) + \Re_1\left(\frac{a k_B T}{\hbar v_L^2 \bar{u}}\right)\right]$	[28]
Bilayer Graphene (BLG)		
Acoustic phonons	$\frac{4m D_{ac}^2 \sqrt{2m E_k}}{\pi \rho \hbar^3 v_s} \int_0^{2k} \frac{(q/2k)^3}{\sqrt{1 - (q/2k)^2}} \frac{g(q, k)}{1 - f(E_k)} \times \left\{ N_q [1 - f(E_k + \hbar \omega_q)] + (N_q + 1) [1 - f(E_k - \hbar \omega_q)] \right\} dq$	[73]
Surface polar optical phonons	$\frac{2mAe^2 F^2}{\pi \hbar^3} \left[(n_q + 1) \int_0^{\varphi_{max}} \frac{1}{ \epsilon(q_{\pm}^e) ^2} \left[\frac{e^{-2q_{\pm}^e d} + e^{-2q_{\pm}^e (d+c)}}{2} \right] \frac{g(q_{\pm}^e) d\varphi}{ 2q_{\pm}^e - 2k } \right. \\ \left. + \left[n_q \int_0^{\pi} \frac{1}{ \epsilon(q_{\pm}^a) ^2} \left[\frac{e^{-2q_{\pm}^a d} + e^{-2q_{\pm}^a (d+c)}}{2} \right] \frac{g(q_{\pm}^a) d\varphi}{ 2q_{\pm}^a - 2k } \right] \right]$	[74]
Coulomb impurities	$\frac{2mn_i}{\pi \hbar^3} \left(\frac{2\pi e^2}{\epsilon}\right)^2 \int_0^{2k} \left(\frac{q}{2k}\right)^2 \frac{g(q, k)}{k [1 - (q/2k)^2]^{1/2}} \frac{dq}{(q + q_{TF})^2}$	[75]
Short range disorder	$\frac{n_d V_0^2 m}{\pi \hbar^3} 2 \int_0^{2k} \left(\frac{q}{2k}\right)^2 \frac{g(q, k)}{k [1 - (q/2k)^2]^{1/2}} dq$	[75]
Armchair Graphene Nanoribbon (AGNR)		
Acoustic phonons	$\frac{2\pi}{\hbar} \sum_{n, k_y} \sum_{q_y} \frac{D_{ac}^2 \hbar q_y }{\rho L W^3 v_s} F_{n, n'} ^2 (1 + \cos(\theta_{n, k_y} - \theta_{n', k_y'})) (1 - \cos(\theta)) \\ \times \Delta(E_{n, k_y}, E_{n', k_y'}) \delta_{q_y, k_y - k_y'}$	[65]
Optical phonons	$\frac{2\pi}{\hbar} \sum_{n, k_y} \sum_{q_y} \frac{D_{op}^2 \hbar}{\rho L W^3 \omega_{LO}} F_{n, n'} ^2 (1 + \cos(\theta_{n, k_y} - \theta_{n', k_y'})) (1 - \cos(\theta)) \\ \times \Delta(E_{n, k_y}, E_{n', k_y'}) \delta_{q_y, k_y - k_y'}$	[65]

Scattering Mechanism	Relaxation Rate, $\tau^{-1}(E)$	Ref.
Edge roughness	$\frac{2\pi}{\hbar} \sum_{n,k_y} \sum_{q_y} \frac{2E_n^2}{L} \frac{H^2}{W^4} \frac{\Lambda}{1+(q_y\Lambda)^2} F_{n,n'} ^2 (1 + \cos(\theta_{n,k_y} - \theta_{n',k'_y})) (1 - \cos(\theta))$ $\times \Delta(E_{n,k_y}, E_{n',k'_y}) \delta_{q_y, k_y - k'_y}$	[65]
Impurities	$\tau_{IMP}^{-1}(E_{n,k_y}) = \frac{2\pi}{\hbar} \sum_{n',k'_y} \sum_{q_y} C_{IMP}(q_y) ^2 (1 + \cos(\theta_{n,k_y} - \theta_{n',k'_y})) (1 - \cos(\theta)) \Delta(E_{n,k_y}, E_{n',k'_y}) \delta_{q_y, k_y - k'_y}$ <p>with</p> $ C_{IMP}(q_y) ^2 = \frac{2}{L^2 W^2} \left(\frac{e^2}{4\pi\epsilon_0 K} \right)^2 \left \int_{-W/2}^{W/2} [\cos(k_n - k_n')x - \cos(\Delta K - k_n - k_n')x] K_0(q_y b) dx \right ^2$	[65]

*Expressions for SG are for $T \gg T_{BG}$

Meanings of symbols (Table 3.):

v_L – Longitudinal sound velocity; v_T – Transverse sound velocity; ρ – mass density

D_{ac} – Acoustic phonon deformation potential constant; D_{op} – Optical phonon deformation potential constant

N_q – Bose-Einstein distribution function with wave vector \mathbf{q}

Δ – rms height; Λ – Correlation length for interface roughness; n_i – Density of charged impurities in the sample;

n_{vac} – Number of vacancies of radius R_o ; $\gamma_i = D(E_F) e^2 / 2 \epsilon \epsilon_0$; ϵ – permeability of substrate

g – Screened deformation potential constant; $\beta = \partial \log t / \partial \log a$, a – Distance between nearest carbon atoms

$\omega_c = a q_c^2$ – Infrared cutoff frequency; $\mathfrak{R}_n(\gamma) = \int_0^\infty dx x^3 / (\gamma^2 x^2 + 1) [\exp(\sqrt{\gamma^2 x^4 + x^2}) - 1]^n$

d – distance between graphene and substrate; $F^2 = (\hbar\omega_s / 2A\epsilon_0) [1 / (\epsilon_s^\infty + 1) - 1 / (\epsilon_s^0 + 1)]$; $\hbar\omega_s$ – energy of SPPs

ϵ_s^∞ (ϵ_s^0) – high (low) frequency substrate dielectric constant,

$g(q, k) = (1 - 2(q/2k)^2)$; $\phi_{\max} = a \cos \sqrt{\hbar\omega_s / E_k}$; $q_\pm^e = k \cos \phi \pm \sqrt{k^2 \cos^2 \phi - \frac{2m\hbar\omega_s}{\hbar^2}}$; $q_\pm^a = -k \cos \phi \pm \sqrt{k^2 \cos^2 \phi + \frac{2m\hbar\omega_s}{\hbar^2}}$

$g(q_\pm^e) = \frac{\sqrt{E_k} - \sqrt{E_{q_\pm^e}} \cos \phi}{\sqrt{E_k - \hbar\omega_s}}$; $g(q_\pm^a) = \frac{\sqrt{E_k} + \sqrt{E_{q_\pm^a}} \cos \phi}{\sqrt{E_k + \hbar\omega_s}}$; $E_{q_\pm^e(a)} = \frac{\hbar^2 q_\pm^e(a)^2}{2m}$;

$q_{TF} = 4me^2 / \epsilon \hbar^2$: Thomas-Fermi screening wavevector; $n_d(V_o)$ – density (strength of potential) of short range impurities.

W – Width of AGNR; L – Length of AGNR;

$|F_{n,n'}|^2 = \left| \left[\frac{\sin(k_n - k_n')(W/2)}{k_n - k_n'} - \frac{\sin(\Delta K - k_n - k_n')(W/2)}{\Delta K - k_n - k_n'} \right] \right|^2$

Ionized impurity atom located at distance $b = [(x-x_o)^2 + (y-y_o)^2 + (z-z_o)^2]^{1/2}$ away from the center of the ribbon

(x_o, y_o, z_o) – Impurity atom position; $N_i(x_o, y_o, z_o)$ – Density of impurities in GNR layer and the substrate.

Table 3. Relaxation rates for various scattering mechanisms in graphene systems

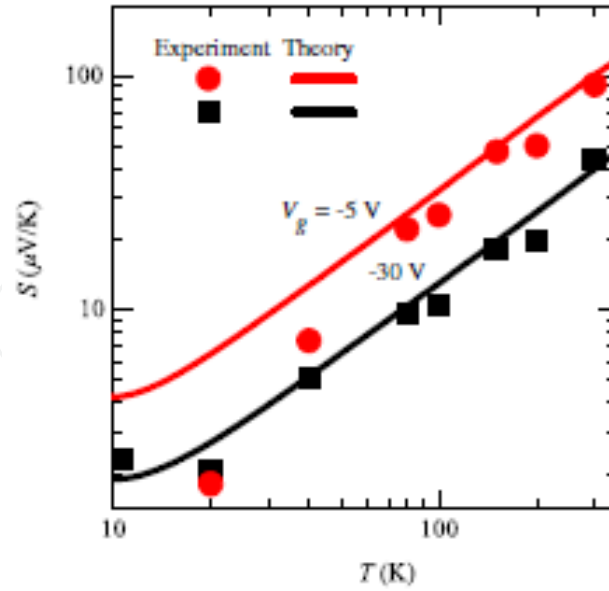


Figure 11. Temperature variation of TEP, $S (= S_d + S_g)$ calculated using balance equation method for $n_s = 2.16 \times 10^{16} \text{ m}^{-2}$ (black curve) and $3.6 \times 10^{15} \text{ m}^{-2}$ (red curve), corresponding, respectively, to $V_g = -30 \text{ V}$ (black squares) and -5 V (red dots) of the experimental data of [16]. (from [77])

Kubakaddi [62] in his study of TEP at low temperatures, has given Mott formula Eq.(36a) for S_d , and predicted the $n_s^{-1/2}$ and linear-in- T dependences. S_d is found to be relatively dominant for $T < 2 \text{ K}$ and $T > 10 \text{ K}$ (see Figure (19)).

Motivated by the experiments of [16], [17] and [18], Hwang *et al* [35] have developed, in the linear response approximation, a theory for the thermopower of graphene, ignoring the drag component. Incorporating the energy dependence of various transport times, they elucidate the comparative importance of scattering mechanisms in graphene. They find that a reasonable explanation for the measured TEP [16-18] can be given by the scattering by random screened charged impurities located in the graphene environment. The density dependence shows the expected $n_s^{-1/2}$ behaviour at high densities. Figure 10 shows the temperature dependence of their calculated TEP for different scattering-time energy-dependence exponents (m). At high temperatures, the TEP is independent of T and approaches a limiting value. Further, the Mott formula is found to apply well, for $T \leq 0.2T_F$ and high carrier densities, but fail in the low-density limit, where electron-hole puddles may dominate and an effective-medium theory may be required.

Considering scattering of electrons by both impurities and phonons, Bao *et al* [77] have studied the behaviour of S_d away from CNP. Within the framework of balance equation approach, they obtain an expression for S_d , which in the limit of large concentrations is shown to reduce to Mott formula. Comparing their calculations of TEP, $S (= S_d + S_g)$ with the data of Zuev *et al* [16] for two values of gate voltage (see Figure 11), they find that for $T > 10 \text{ K}$, S_d plays an essential role and the TEP shows a linear dependence on T .

Vaidya *et al* [63] have studied S_d for $30 < T < 300 \text{ K}$, using Eq.(33) and considering the electrons to be scattered not only by phonons [50, 66] but also other disorder-related scattering mecha-

nisms namely, charged impurities *via* long-range Coulomb interaction [72], the vacancies [72] in the system and surface roughness [66] arising from the rippling of the graphene sheet deposited on oxidized Si substrate (see Figure (12)). S_d is found to increase almost linearly with temperature, determined mainly by vacancy and impurity scatterings. In the case of the scattering of electrons by non-polar optical phonons *via* deformation potential coupling, although the emission of optical phonons is possible only if the kinetic energy of carriers exceeds $\hbar\omega_{LO}$, this mechanism could become important for higher energy carriers. For $n_s = 2 \times 10^{16} \text{ m}^{-2}$, a value realized in the sample of Zuev *et al* [16], $E_F = 135 \text{ meV}$, and the onset of optical phonon emission is only a few $k_B T$ times greater than E_F . A departure from linear T -dependence due to optical phonons is noticed (Figure 12a) and, as a function of carrier concentration, a change in the sign of $|S_d|$ is observed. Their analysis, assuming S_g to be negligible, obtains a fit with $S(T)$ data of Zuev *et al* (Figure 12b).

The effect of electron-phonon scattering processes on TEP of extrinsic graphene has been studied by Munoz [78]. From a variational solution of the Boltzmann equation, he obtained analytical expressions for the transport coefficients and the leading contribution to phonon-limited TEP. Figure 13 represents his results of temperature dependence of TEP at different electronic densities. At lower temperatures ($T < \sim 60 \text{ K}$), TEP is found to show a linear in T dependence (see inset of Figure 13) and to reproduce the $n_s^{-1/2}$ dependence with carrier density, in agreement with reported experimental data [17].

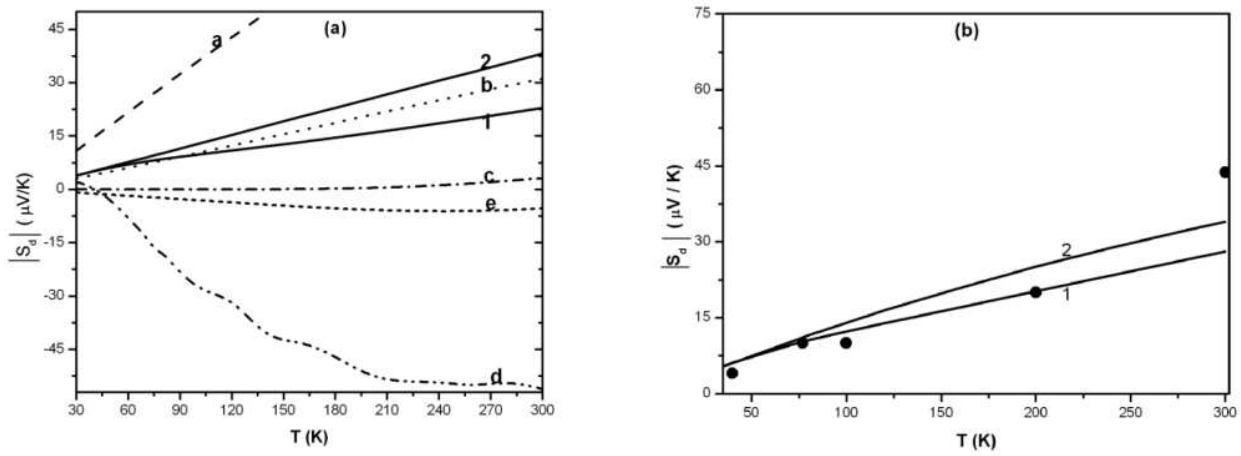


Figure 12. Temperature dependence of the S_d calculated using Eq. (33) for SLG with $n_s = 2 \times 10^{16} \text{ m}^{-2}$. (a) Dashed, dotted, dash-dotted, short-dashed and dash-double-dotted curves represent individual contributions from impurities, vacancies, acoustic phonons, surface roughness and optical phonons, respectively. Curve 1 represents the overall contribution. Curve 2 represents the variation of S_d according to the Mott expression (36a). (b) Comparison of calculations (curves) with the experimental data of [16] (dots). Curves 1 and 2 represent calculations using Eqs. (33) and (36a) respectively. (from [63])

The distinctive features observed in the energy dependence of the relaxation times $\tau(E_k)$ of the scattering mechanisms in graphene are clearly exhibited in the case of the intrinsic acoustic phonon scattering in the Bloch-Gruneissen (BG) regime, where acoustic phonon scattering dominates and phonon energies are approximately of the order of thermal energy ($\hbar\omega_q \sim k_B T$). In their experimental study of the resistivity of graphene, Efetov and Kim [68] have demon-

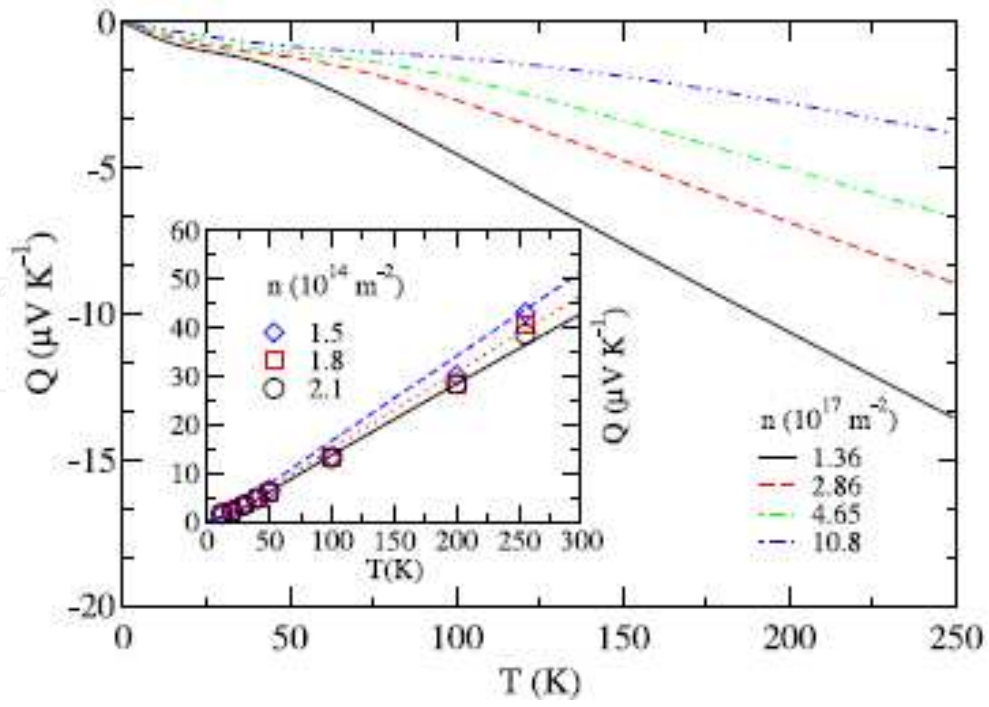


Figure 13. Temperature dependence of TEP at different electronic densities, n . Inset: Comparison with data of [17] at corresponding hole densities.(from [78]).

strated that the transition from higher temperature into the BG regime is reflected by a change in the character of electron scattering by acoustic lattice vibrations. With a view to examine the influence of the changed character of electron scattering on S_d , Sankeshwar *et al* [71] first study the behaviour of acoustic phonon limited scattering rates, $\tau^{-1}(E_k)$ in SLG for $T < T_{BG}$. For a graphene sample with $n_s=10^{16}\text{m}^{-2}$, $T_{BG} \sim 60$ K. Figure 14.(a) shows the strong influence this change has on the energy dependence of the unscreened electron-phonon interaction momentum relaxation times, τ_{BG}^{-1} around $E = E_F$. The sharp decrease in τ_{BG}^{-1} at $E = E_F$ for $T = 4.2\text{K}$ is due to the factor $\Delta(E_k, E_k)$ in Eq. (38), governing probability occupation factors of electrons and phonons. With increase in the temperature from 4.2K to 77K to 300 K, the extent of the dip in τ_{BG}^{-1} at E_F is seen to decrease and gradually disappear at higher temperatures, as also the difference between the magnitudes of the rates τ_{BG}^{-1} and τ_{EP}^{-1} , the momentum relaxation time in the EP approximation.

In their investigation of the temperature dependence of S_d in the BG regime, Sankeshwar *et al* have shown that, corresponding to the transition into BG regime, S_d exhibits a non-linear temperature dependence (dotted curve in Figure 14. (b)) before becoming linear at very low temperatures [71]. Such dependence is also exhibited in conventional 2D systems [79]. The minimum value of $|S_d|$ occurs around $T = T_{BG}$ and a change in the sign of $|S_d|$ is also noticed (dotted curve in Figure 14. (b)). On the other hand, the variation of $|S_d|$ in EP regime, calculated using Eq. (31), (38) and (39c) is found to be almost linear for $T > T_{BG}$, eventually merging with $|S_d|$ at higher temperatures [71].

The influence that S_d can have on the behavior of total TEP, S ($= S_d + S_g$), is illustrated in Figure 14.(b). The dashed curve depicts S_g , calculated in phonon-boundary scattering limit with $\tau_p = \Lambda / v_s$ for $n_s = 1 \times 10^{16} \text{ m}^{-2}$ and phonon mean free path, $\Lambda = 100 \text{ nm}$, and curve 1 represents S . Here, S_g being small for $T < 25 \text{ K}$, the overall TEP, S , exhibits the nonlinear temperature dependence of S_d in the BG regime ($T < 60 \text{ K}$), whereas for higher temperatures, is influenced by S_g . A comparison of curve 1 with curves 2 ($\Lambda = 500 \text{ nm}$) and 3 ($\Lambda = 1000 \text{ nm}$), shows that an increase in Λ leads to not only an increase in magnitude of S but also a change in its behavior in the BG regime. It is seen from Figure 14.(b) that the non-linear structure of S , exhibited due to S_d for smaller Λ , is masked by S_g for larger Λ . The electrostatic tunability of the chemical potential, $E_F = \hbar v_F k_F$, in graphene allows for a wide range of control of T_{BG} and could therefore, with proper control of S_g , allow the non-linear behavior of S_d to be observed. Figure 14.(c) shows comparison of the calculations for $\Lambda = 200 \text{ nm}$, with experimental data of Wei *et al* [17]. The deviation from data for higher temperatures suggests possible influence of other electron and phonon scattering mechanisms operative in real systems [33, 80], and calls for more detailed investigations.

Mariani and Oppen [67] and Ochoa *et al* [28], in their investigations of the resistivity of suspended SLG and BLG, have studied the effect of strain. They show that in the absence of strain, the FPs dominate the phonon contribution to resistivity, whereas in the presence of strain, the contribution due to FPs is suppressed and the in-plane phonon modes become dominant. These features seen in the scattering rates get reflected in the TE properties [81, 82]. Vaidya *et al* [81] have investigated the acoustic phonon limited S_d of suspended SLG, considering contributions from both in-plane and flexural acoustic phonons. Restricting their analysis to scattering in SG with high electron densities, in EP regime ($60 < T < 300 \text{ K}$), they study the role of strain in influencing the total TEP, S . Figure 15.(a) shows the temperature dependence of TEP of a SG with $n_s = 1 \times 10^{16} \text{ m}^{-2}$ [81]. The dominant contribution to S is from the phonon drag component, S_g for $T < 90 \text{ K}$, in the absence as well as presence of strain. However, for higher temperatures ($T > 150 \text{ K}$) the contribution from S_d becomes important. The effect of strain, which is known to suppress the electron-FP interaction [28], is found to suppress S_d and to alter its behavior, the effect being larger at higher temperatures. The total diffusion TEP due to both in-plane (I) and flexural (F) phonons is calculated taking the overall momentum relaxation rates to be given by Matthiessen's rule: $\tau_{ns}^{-1} = \tau_I^{-1} + \tau_F^{-1}$, for non-strained SG, and $\tau_s^{-1} = \tau_I^{-1} + \tau_{F, str}^{-1}$, for strained SG. Figure 15.(b) shows the fit obtained with the calculations of S_d (curves 1 and 2) by Vaidya *et al* [82] for the data (dots) of suspended unstrained Cu-CVD SLG sample of Xu *et al* [45], for which, as suggested by thermal conductivity measurements, most of the heat is carried by FPs in the absence of strain. The almost linear temperature dependence suggests that the major contribution to TEP for $T < 170 \text{ K}$ is due to the diffusion component, as observed by Xu *et al* [45]. The deviation for $T > 170 \text{ K}$, from experimental data, suggests the role of additional scattering mechanisms.

Apart from those mentioned above, there have been reports of other related TEP studies. The investigations of Sharapov and Varlamov [83] and Patel and Mukerjee [84], with regard to the effect of opening a gap in the graphene spectrum, find that the TEP is found to be proportional to the band gap. Zhou *et al* [85] have studied dependence of TEP on the polarization strength

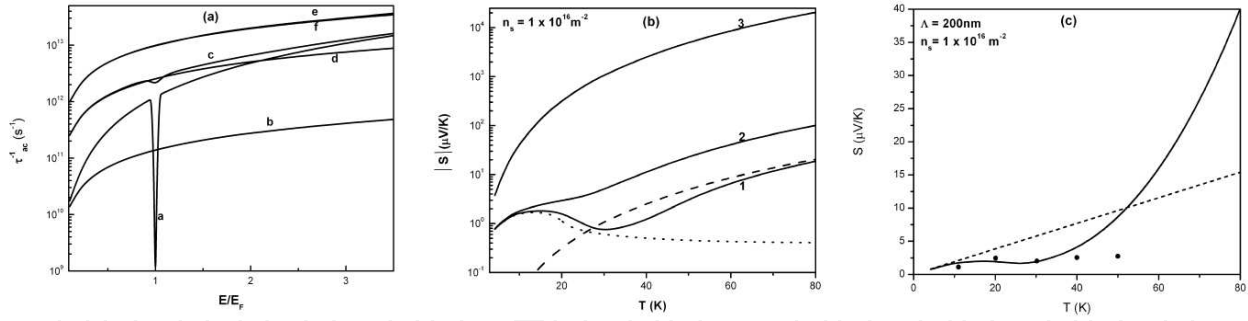


Figure 14. (a) Variation of acoustic phonon limited rates, τ_{BG}^{-1} and τ_{EP}^{-1} , as function of carrier energy E in SLG with $n_s = 10^{16} \text{ m}^{-2}$. Curves a, c, and e depict variation of τ_{BG}^{-1} for $T = 4.2, 77$ and 300 K respectively. Curves b, d and f depict the temperature variation of τ_{EP}^{-1} . (b) Temperature dependence of acoustic phonon limited S_d (dotted curve), S_g (dashed curve, with $\Lambda = 100 \text{ nm}$) and overall TEP, S (curve 1) of SLG with $n_s = 1 \times 10^{16} \text{ m}^{-2}$. Curves 2 and 3 depict S for S_g with $\Lambda = 500$ and 1000 nm , respectively. (c): Comparison of calculated S for $\Lambda = 200 \text{ nm}$ (full curve) and Mott S_d (dashed curve) with data of [17] for $V_g = 50 \text{ V}$ (dots). (from [71])

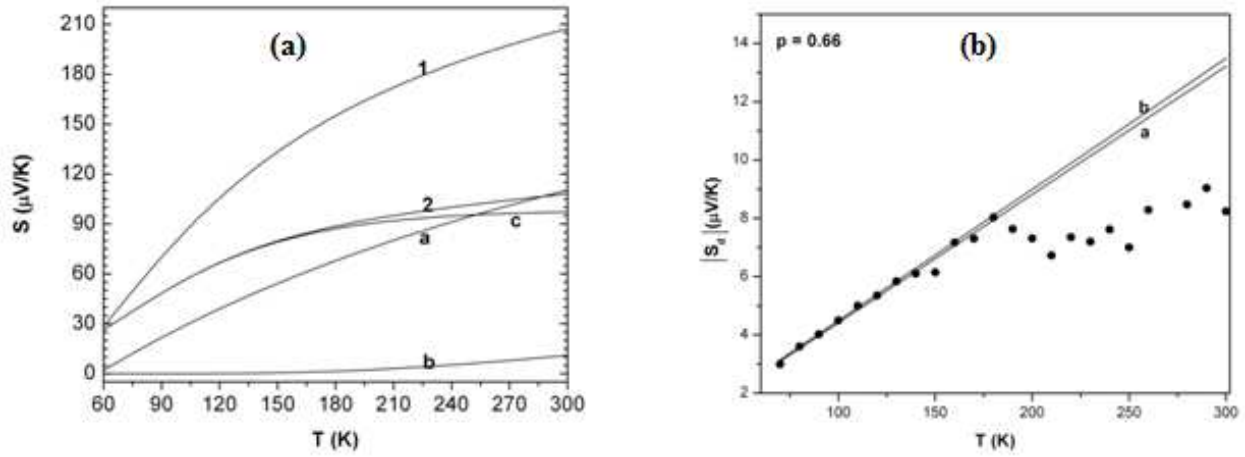


Figure 15. Temperature dependence of acoustic phonon limited TEP of suspended SLG. (a). Curves a and b represent S_d calculated using Eq. (33) using $n_s = 1 \times 10^{16} \text{ m}^{-2}$ for non-strained and strained samples, respectively. Curve c depicts S_g . Curves 1 and 2 represent $S (= S_d + S_g)$ in non-strained and strained samples, respectively. (b) Comparison of calculations of S_d for $n_s = 1 \times 10^{17} \text{ m}^{-2}$ with data (dots) of [45]. Curves 1 and 2 depict, S_d due to FPs calculated using Eq. (32) and (36a) (from [81], [82])

of ferromagnetic leads, and find TEP to depend weakly on the strength and the magnetic configuration of the system.

3.3.2. Diffusion thermopower in BLG

In the last few years, TEP in BLG has been studied both theoretically [64, 86] and experimentally [49]. Nam *et al* [49] find the low- T TEP of BLG with large n_s , to follow the Mott relation with a linear-in- T dependence, suggesting a weak electron-phonon interaction. Hao and Lee [86], in their theoretical investigation, have studied the temperature and carrier density dependence of TEP of gapped relatively clean BLG in terms of the Kubo formula, with impurity scattering treated in the self-consistent Born approximation. They find that introducing a gap enhances the TEP.

Kubakaddi and Bhargavi [64, 73] give an expression for S_d , and compare their calculations of S_d with the data of Nam *et al* [49]. Figure 16.(a) shows the T dependence of S_d calculated taking into account the contributions from acoustic phonons (APs) *via* deformation potential coupling [73], surface polar phonons (SPPs) [74], charged impurity (CI) and short range disorder (SD) [75]. Although the contributions from SPPs (for $T < \sim 200$ K) and the APs (for $T < \sim 20$ K) exhibit non-monotonic behavior, the overall contribution is found to show almost linear temperature dependence. The non-linear T variation due to APs is attributed to the dip arising around $E=E_F$ in the energy dependence of the carrier relaxation time (as in Figure 14.(a) for SLG). Their calculations of S_d for parameters characteristic of the samples of Nam *et al* [49] obtain a qualitative agreement with data (see inset in Figure 16.(a)). Figure 16.(b) shows the carrier density dependence of S_d at $T = 300$ K. Although the dependence for SPPs is $S_d \sim n_s^{-0.75}$, the overall S_d is found to show almost $S_d \sim n_s^{-1}$ behavior. This inverse dependence of S_d on n_s is unlike $\sim n_s^{-1/2}$ dependence observed for SLG but similar to that for degenerate conventional 2DEG [11]. Detailed investigations of TEP in BLG over wider temperature ranges are required to better understand the contribution of S_d relative to that of S_g ; they are found to be similar (see Figure (22)).

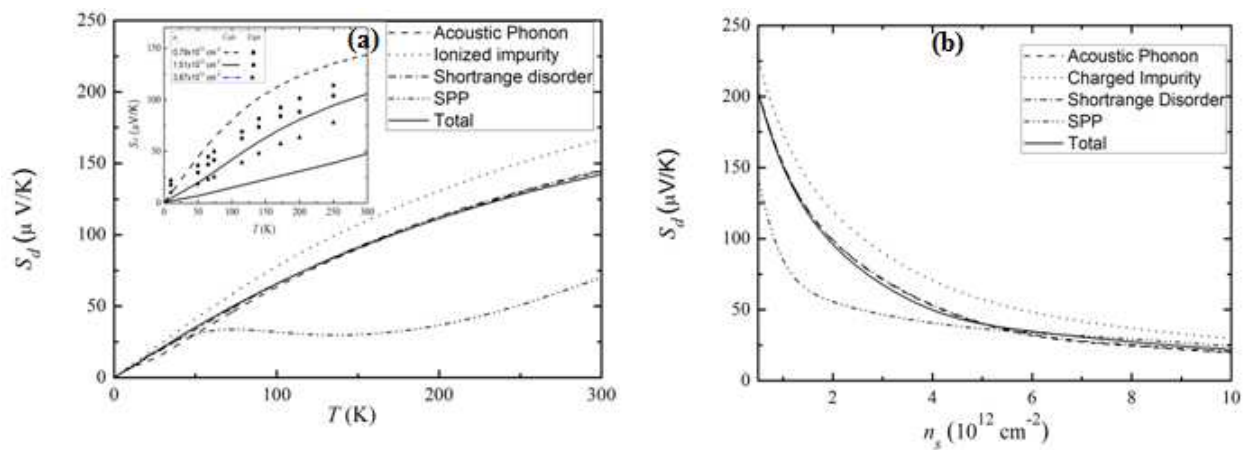


Figure 16. Variation of S_d of BLG as a function (a) T with $n_s = 1 \times 10^{12} \text{ cm}^{-2}$, and (b) n_s , at $T = 300$ K. Inset in (a) shows T dependence of S_d calculated for sample of [49]. (from [73])

In the case of suspended BLG, S_d is found to be enhanced [73]. However, the behavior of S_d considering contributions from APs and CI, is found to be same as for supported BLG.

3.3.3. Diffusion thermopower in AGNR

The theoretical efforts, to understand the diffusion contribution to TEP of GNRs have been based on different techniques. Divari and Kliros [87] have studied TEP of ballistic wide graphene ribbons with aspect ratio ($W/L \geq 3$) using linear response theory and the Landauer formalism. Xing *et al* [88] have studied TEP of GNRs in zero and non-zero magnetic field using non-equilibrium Green's function technique and shown that TEP depends on the chirality of the GNR. The TE properties have also been investigated by solving the electron and phonon transport equations in the nonequilibrium Green's function formalism [7, 89-91]. With a view

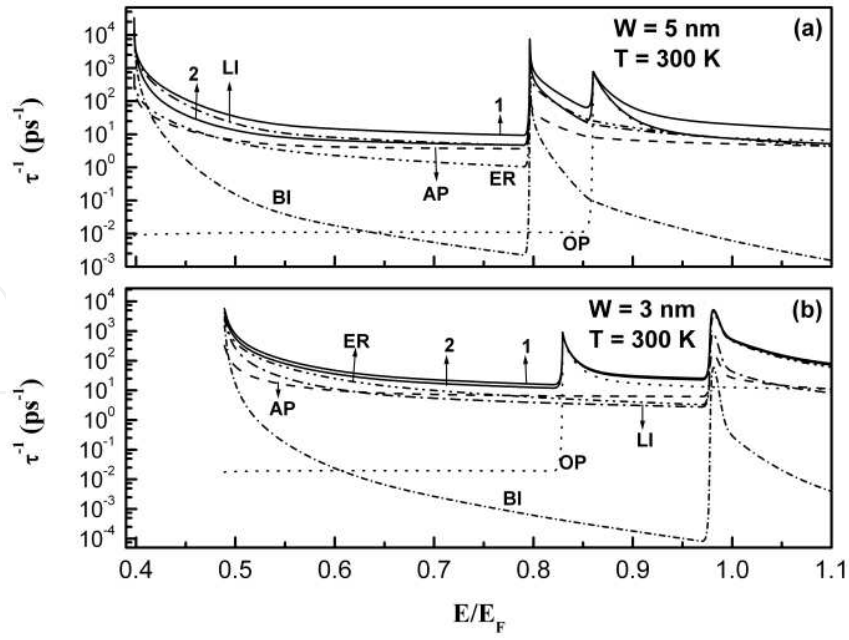


Figure 17. Energy dependence of relaxation rates for AGNRs of widths (a) 5 nm, and (b) 3 nm, with $n_i = 5 \times 10^8 \text{ m}^{-1}$ at $T = 300 \text{ K}$. Dash-double-dotted, dash-dotted, short-dash dotted, dashed and dotted curves, respectively, represent contributions from ER, LI, BI, AP and OP scatterings. Curves 1 and 2, respectively denote overall relaxation rates τ_1^{-1} and τ_2^{-1} , given in the text. (from [65])

to achieve a high TE figure of merit, Mazzamato *et al.* [92] in their recent study of the TE properties of GNRs have proposed optimized patterning of the ribbons with regard to their width and edge orientations.

Recently, in their systematic study of S_d of semiconducting AGNR systems employing Boltzmann formalism, Nissimagoudar and Sankeshwar [65] have illustrated the relative importance of various electron scattering mechanisms, and studied the influence of GNR width and subband structure on the behavior of S_d . Considering the electrons to be scattered by edge roughness (ER), impurities (IMPs) and deformation-potential coupled acoustic phonons (APs) and optical phonons (OPs), they obtain expressions for the relaxation times, $\tau_j^{-1}(E_k)$, for $j \equiv \text{AP, OP, ER, IMP}$ (see Table 3). Owing to the peculiar nature of the density of states, the energy dependences of the momentum relaxation times, unlike as in the case of SLG (see Figure 14.(a)), exhibit distinctive features as depicted in Figure 17 for AGNRs with $n_i = 5 \times 10^8 \text{ m}^{-1}$, for $T < 300 \text{ K}$. Two peaks, one corresponding to the subband and the other due to OP emission, are observed. The dominant contribution to the overall rate $\tau_1^{-1} = \tau_{ER}^{-1} + \tau_{LI}^{-1} + \tau_{AP}^{-1} + \tau_{OP}^{-1}$ (curve 1) is from LI scattering (impurities in the graphene layers only), the contribution from AP scattering being less. Assuming the impurities to be distributed uniformly not only in the layer but also in the substrate, the overall rate $\tau_2^{-1} = \tau_{ER}^{-1} + \tau_{BI}^{-1} + \tau_{AP}^{-1} + \tau_{OP}^{-1}$ (curve 2) is found to be dominated by ER scattering indicating that the contribution from the IMPs in the substrate is small [27]. The rates for a AGNR with $W = 3 \text{ nm}$ (shown in Figure 17.(b)) are found to exhibit the same features as seen for $W = 5 \text{ nm}$ (Figure 17.(a)), however, with a corresponding shift in the positions of the two peaks. In this case, it may be noted that the onset of OP emission occurs before the occupation of the second subband.

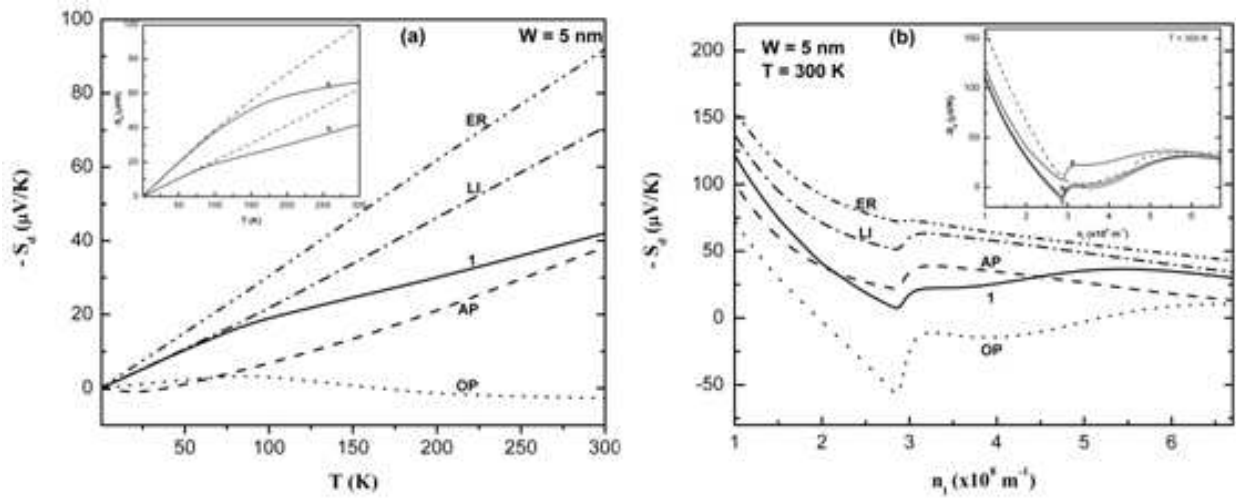


Figure 18. Variation of S_d of an AGNR of $W= 5$ nm, with (a) temperature for $n_i = 2 \times 10^8 \text{ m}^{-1}$, and (b) linear carrier density at $T=300$ K. Curve 1 denotes overall contribution to S_d , calculated using τ_1^{-1} given in text, from scatterings due to ER (dash-double-dotted curve), LIs (dash-dotted curve), APs (dashed curve) and OPs (dotted curve). The inset in (a) shows overall S_d calculated using τ_1^{-1} for two AGNR widths: 3 nm (curve a) and 5 nm (curve b). Dashed curves show the overall S_d according to Mott expression. The inset in (b) shows overall S_d for an AGNR of width 5 nm for three values of LI concentrations, n_s : 10^{14} m^{-2} (curve a), 10^{13} m^{-2} (curve b), and 10^{12} m^{-2} (curve c). Dashed curve shows overall S_d for AGNR of $W= 3$ nm, with $n_s = 10^{14} \text{ m}^{-2}$. (from [65])

The above mentioned changed energy dependences of the relaxation times are found to influence the behavior of and lead to distinctive features in S_d as shown in Figure 18. The temperature dependence of the overall S_d (curve 1 in Figure 18.(a)), for an AGNR of width 5 nm, supporting an electron density $2 \times 10^8 \text{ m}^{-1}$, is found to be almost linear up to $T \sim 75$ K, the dominant contribution being from LI scattering. At higher temperatures, the contribution due to OP scattering becomes increasingly important and S_d is found to exhibit room temperature value of $42 \mu\text{V/K}$. A decrease in the GNR width (to $W= 3$ nm), is found not only to enhance the magnitude of S_d but also alter its behavior (depicted by curve a in inset of Figure 18.(a)) due to the changed temperature and energy dependences of the individual contributions. Figure 18.(b) illustrates the influence of subband structure on room temperature S_d for an AGNR of width 5 nm. As a function of carrier density, S_d shows a step-like behavior, increasing in magnitude, when Fermi energy moves into the second subband, and reflects the singular nature of the AGNR density of states.

With a proper choice of parameters characterizing the extrinsic scattering mechanisms, and the possibility of modulating the Fermi level with a control on gate and bias voltages [93], the behavior of overall S_d in AGNRs could, therefore, be tuned and the subband structure in S_d be detected. Further, the enhancement in S_d with a decrease in the ribbon width, portends promising applications in thermoelectric devices.

4. Phonon-drag thermopower in graphene systems

As mentioned in section 2, in the presence of temperature gradient ∇T , the flow of phonons carries a momentum current, a fraction of which is transferred to electrons via phonon-electron interaction, giving rise to the phonon-drag component, S_g . S_g , unlike the diffusion contribution, depends only on the electron-acoustic phonon coupling strength. It has been extensively studied in conventional semiconductor 2DEG [11, 94, 95]. As recent observations of very large thermal conductivity in graphene [96-98] suggest the phonon mean free path Λ to be large, S_g , which also depends on the phonon mean free path Λ , is expected to be large in graphene systems. Λ in a system is decided by the various phonon-scattering mechanisms operative in it.

The formal theory of S_g , based on the semi-classical Boltzmann formalism, has been developed for a conventional 2DEG coupled to 3D phonons in semiconductor heterostructures [99]. With appropriate modifications, Kubakaddi [62, 64, 100] have applied it to graphene systems. The coupled Boltzmann equations for electrons and phonons are solved and the current density due to phonon-drag is obtained. The 2D electrons are assumed to interact with the in-plane 2D LA phonons of energy $\hbar\omega_q$ with $\omega_q = v_s q$, and $\mathbf{q} = (q_x, q_y)$ is the 2D phonon wave vector. For the electron-acoustic phonon interaction *via* unscreened deformation potential coupling, S_g is given by

$$S_g = \frac{2e}{A\sigma k_B T^2} \sum_{\mathbf{k}, \mathbf{k}', \mathbf{q}} \hbar\omega_q f(E_{\mathbf{k}}) [1 - f(E_{\mathbf{k}'})] P_q^a(\mathbf{k}, \mathbf{k}') \tau_p \mathbf{v}_p \cdot (\mathbf{v}_{\mathbf{k}} \tau_{\mathbf{k}} - \mathbf{v}_{\mathbf{k}'} \tau_{\mathbf{k}'}) \quad (40)$$

where $\mathbf{v}_p = v_s \mathbf{q}/|\mathbf{q}|$ is the phonon group velocity, $\tau_{\mathbf{k}}$ ($\tau_{\mathbf{q}}$) is the electron (phonon) momentum relaxation time. The transition rate, $P_q^a(\mathbf{k}, \mathbf{k}')$, at which the electron in state \mathbf{k} makes transition to state \mathbf{k}' by absorbing a phonon, is given by

$$P_q^a(\mathbf{k}, \mathbf{k}') = \frac{2\pi}{\hbar} |C(q)|^2 F(\theta) N_q \delta(E_{\mathbf{k}'} - E_{\mathbf{k}} - \hbar\omega_q) \delta_{\mathbf{k}', \mathbf{k}+\mathbf{q}}. \quad (41)$$

The phonon-drag is known to be important at low temperatures [8, 9, 11, 94, 95]. At these temperatures the phonon scattering is dominated by boundary scattering and $\tau_p = \Lambda/v_s$, with Λ corresponding to smallest linear dimension of the sample.

4.1. Phonon-drag thermopower in SLG

Kubakaddi has studied in detail the low-temperature behavior of S_g . The low temperature S_g in the boundary scattering regime, can be expressed as [62]

$$S_g = -\frac{D_{ac}^2 \Lambda}{2\pi\rho e E_F k_B T^2 \hbar^2 v_s^3 v_F} \int_0^\infty dq \int_\gamma^\infty dE_{\mathbf{k}} (\hbar\omega_q)^3 \sqrt{1 - (\gamma/E_{\mathbf{k}})^2} N_q f(E_{\mathbf{k}}) [1 - f(E_{\mathbf{k}} + \hbar\omega_q)], \quad (42)$$

where $\gamma = \hbar v_F q/2$. Figure 19 shows that the low temperature dependence of S_g calculated using Eq.(42), with $D_{ac} = 19$ eV and $\Lambda = 10 \mu\text{m}$ [101] for three values of n_s , is similar to that of conventional 2DEG [11]. Also shown (dotted curve) is the temperature dependence of S_d obtained from Mott formula (Eq. 36a) with $p=1$ for $n_s=1.0 \times 10^{12} \text{cm}^{-2}$. The relative magnitudes of S_g and S_d depend upon the values of D_{ac} , Λ , n_s , T and p . S_g is found to be not negligible, contrary to the earlier qualitative remarks [35]. A system, for which S_d could be made to vanish (say, with $p = -1$) will be suitable for study of S_g and to estimate D_{ac} .

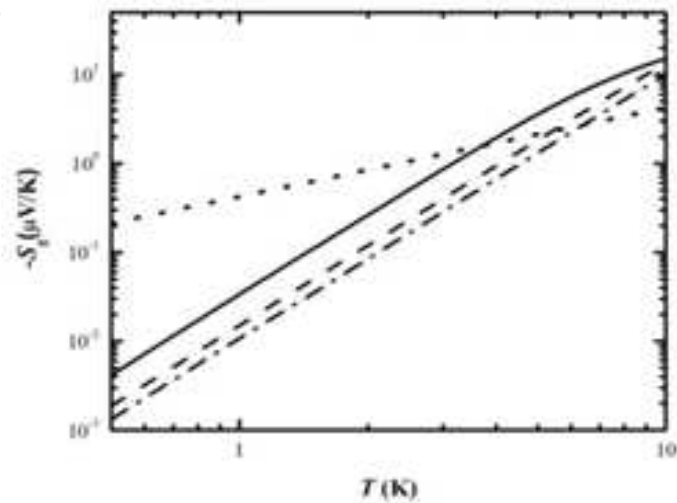


Figure 19. S_g as a function of T for $n_s = 1.0 \times 10^{12} \text{ cm}^{-2}$ (solid curve), $n_s = 5.0 \times 10^{12} \text{ cm}^{-2}$ (dashed curve) and $n_s = 10.0 \times 10^{12} \text{ cm}^{-2}$ (dot-dashed curve). Dotted curve represents S_d , with $p=1$, for $n_s = 1.0 \times 10^{12} \text{ cm}^{-2}$. (from [62])

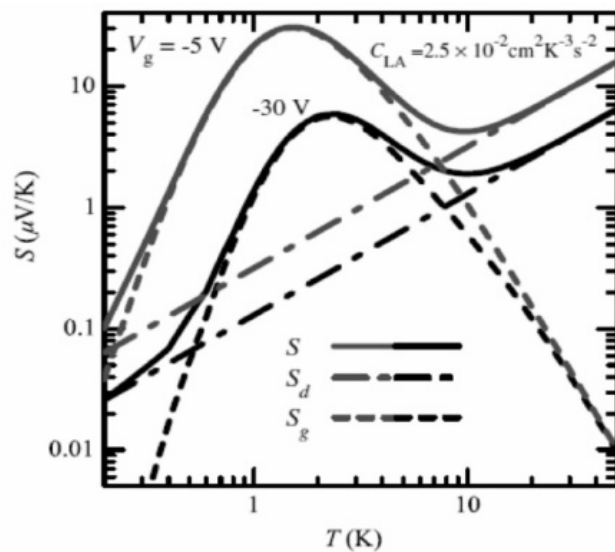


Figure 20. Temperature dependence of S_g , S_d and $S (= S_g + S_d)$ of SLG for $n_s = 2.16 \times 10^{12} \text{ cm}^{-2}$ ($V_g = -5 \text{ V}$), $n_s = 3.6 \times 10^{11} \text{ cm}^{-2}$ ($V_g = -30 \text{ V}$). (from [77]).

Taking account of boundary scattering as well as phonon-phonon interaction in the phonon relaxation processes, Bao *et al* [77] have given the theory of S_g , using balance equation approach. Covering a larger range of temperature, they find (Figure 20) that S_g is important for $T < 10$ K and that the phonon-phonon interaction leads to a peak in its T dependence. The dash-dotted curve represents S_d considering scattering of electrons by impurities and phonons. The main contribution to TEP is mainly due to S_d for $T > 10$ K.

In the BG regime, Kubakaddi gives a simple power law for S_g [62]:

$$S_g = S_{g0} T^3 \quad (43)$$

where S_{g0} ($= S_{g0}^{(SLG)}$) $= -[D_{ac}^2 \Lambda k_B^4 4! \zeta(4)] / [2\pi e \rho E_F \hbar^3 v_s^4 v_F]$ and $\zeta(n)$ is the Riemann zeta function. The cubic T dependence of S_g is a characteristic of 2D nature of phonons and is in contrast to the $S_g \sim T^4$ dependence of unscreened deformation potential scattering in conventional 2DEG [11, 94, 99, 102]. The inverse dependence of S_g on E_F suggests $S_g \sim n_s^{-1/2}$ in contrast to $n_s^{-3/2}$ in conventional 2DEG [11, 94]. This n_s dependence of S_g may be verified experimentally in graphene as it is possible to control n_s experimentally, say through the applied gate voltage.

In conventional 2DEG, in the BG regime, S_g and phonon limited mobility μ_p are known to be related by Herring's formula: $S_g \mu_p \sim T^{-1}$, first given for bulk semiconductors [9, 94, 103, 104]. Since in 2D graphene $\mu_p \sim T^{-4}$ [50], Eq.(43) gives $S_g \mu_p = -v_s \Lambda T^{-1}$ [62] so that Herring's law is validated even in 2D graphene, in which 2D electrons with linear dispersion interact with 2D phonons with $\omega_q \sim q$. This relation can, therefore, be used to determine, as in 2D GaAs system [105], a value for μ_p , from the measured S_g . It may be mentioned here that for the 2D phonons with $\omega_q \sim q^2$ (flexural modes) in semiconducting thin films, Herring's law is shown to be invalidated [106].

A useful and simple approach to calculate S_g is from the force balance argument that $S_g \propto -f C_v / n_s e$ [11], where C_v is the lattice specific and f is the fraction of momentum lost by the phonons to the carriers. At very low T , $C_v \sim T^2$ for 2D phonons in graphene giving approximately $S_g \sim T^2$ [62] in contrast to $S_g \sim T^3$ for 3D phonons [11].

4.2. Phonon-drag thermopower in BLG

The theory of S_g in BLG has been developed by Kubakaddi and Bhargavi [64] in the phonon-boundary scattering regime, at low T . Its expression is given by

$$S_g = - \frac{m^{3/2} D_{ac}^2 \Lambda}{2^{3/2} n_s e k_B T^2 \rho \pi^2 (\hbar v_s)^4} \int_0^\infty d(\hbar \omega_q) (\hbar \omega_q)^3 \int_{E_q}^\infty dE_k F(E_k, \omega_q) N_q \frac{f(E_k) [1 - f(E_k + \hbar \omega_q)]}{\sqrt{E_k - E_q}}, \quad (44)$$

where $E_q = (\hbar^2/2m)[(q/2) - (mv_s/\hbar)]^2$ and $F(E_k, \omega_q) = [1 - (\hbar \omega_q)^2/4mv_s E_k]^2$ is the function due to the chiral character of the carriers. Setting $F(E_k, \omega_q) = 1$, Eq.(44) gives $S_g = S_{g, 12D}$ for the ideal 2D system (with no chiral character of electrons).

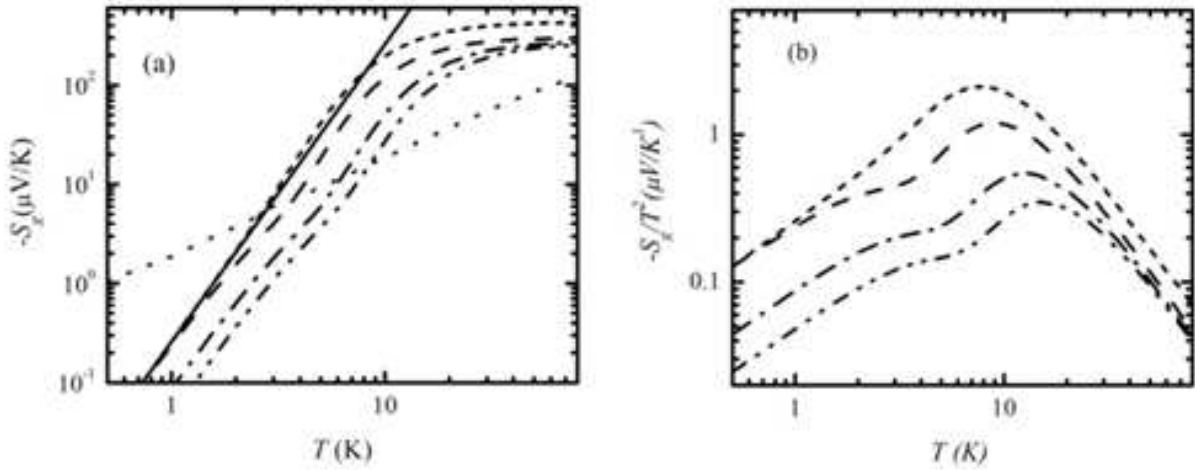


Figure 21. Temperature dependence of (a) S_g and (b) S_g/T^2 for $\Lambda=10 \mu\text{m}$ and $D=20 \text{ eV}$. Dashed curve is for $n_s=0.5 \times 10^{12} \text{ cm}^{-2}$; dash-dotted curve is for $n_s=1.0 \times 10^{12} \text{ cm}^{-2}$; and dot-dot-dashed curve is for $n_s=1.5 \times 10^{12} \text{ cm}^{-2}$. Dotted curve is due to S^d for $n_s=0.5 \times 10^{12} \text{ cm}^{-2}$, $n_i=1 \times 10^{11} \text{ cm}^{-2}$ and $n_d V_o^2=2 \text{ (eV\AA)}^2$. Short dashed curve is due to S_g with $F(E_k, \omega_q)=1$ for $n_s=0.5 \times 10^{12} \text{ cm}^{-2}$ and solid curve is due to S_g for $n_s=0.5 \times 10^{12} \text{ cm}^{-2}$ in the BG regime. (from [64])

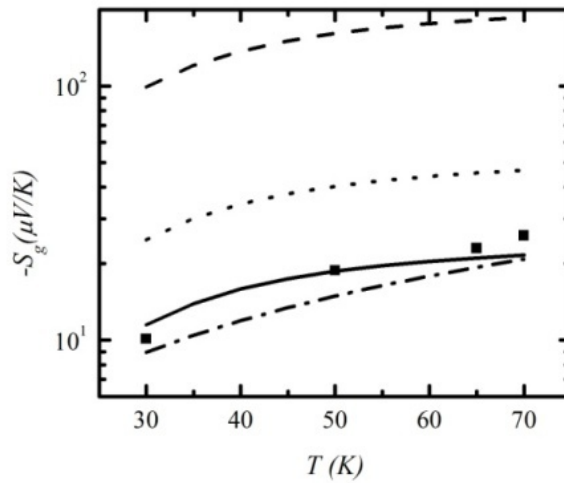


Figure 22. S_g as a function of T for BLG sample of [49] with $\Lambda=8.8 \mu\text{m}$ and $n_s=3.67 \times 10^{12} \text{ cm}^{-2}$ for $D_{ac}=6.8 \text{ eV}$ (solid curve). $D_{ac}=20 \text{ eV}$ (dashed curve), $D_{ac}=10 \text{ eV}$ (dash-dotted curve). Dotted curve represents S_d for $n_i=1 \times 10^{11} \text{ cm}^{-2}$, $n_d V_o^2=2 \text{ (eV\AA)}^2$. Closed squares are experimental data of [49]. (from [64])

Figure 21 shows the temperature dependence of S_g calculated using Eq.(44) [64]. Starting with T^3 at very low T , S_g gradually changes in to sublinear behavior in higher T region, and then flattens, thereby producing a knee. Inclusion of scattering due to Umklapp processes and point defects in the phonon relaxation time is expected to induce a peak at larger T , as found in the behavior of S_g of carbon nanotube [107] and of thermal conductivity of SLG [97]. Such an inclusion obtained good fits with data in the case of conventional 2D systems [108]. The dotted curve in Figure 21.(a) represents S_d , calculated using Eq.(36a), for $n_s=0.5 \times 10^{12} \text{ cm}^{-2}$ assuming

scattering by ionized impurities (with concentration n_i) and short-range disorder (of strength $n_d V_o^2$).

Kubakaddi and Bhargavi [64] have studied the influence on S_g of the form factor $F(E_k, \omega_q)$ in Eq.(44), arising from the chiral nature of the electrons, It is shown to produce a kink in the curves of S_g/T^2 vs T around 6 K (Figure 21(b)). The dashed curve corresponding to $F(E_k, \omega_q) = 1$, for ideal 2D, does not show such a kink. The effect of chiral character is shown to vanish in the BG regime and reduce the range of T for validity of BG regime. In the higher T regime the chiral nature is shown to reduce the magnitude of S_g , as compared to that of ideal 2DEG, S_{g12D} , and the reduction is T dependent.

Nam *et al* [49], from their experimental investigations of TEP of a BLG sample for different n_s , for $30 < T < 250$ K, find that the low- T TEP can be explained by Mott formula. However, Kubakaddi and Bhargavi [64] show that the low- T ($30 < T < 70$ K) data of [49] can be explained by S_g alone by varying D_{ac} . Figure 22 shows the fit to the data for $n_s = 3.67 \times 10^{12} \text{ cm}^{-2}$.

In BG regime, S_g can be described by Eq.(44), but with $S_{g0} (= S_{g0}^{(BLG)}) = -[m^2 D_{ac}^2 \Lambda k_B^4 4! \zeta(4)] / [2\pi^{5/2} e \rho n_s^{3/2} \hbar^2 (\hbar v_s)^4]$. It may be noted that $S_g \sim T^{-3}$ is a manifestation of the 2D phonons, as in SLG, in contrast with the T^{-4} dependence in conventional 2D systems [102]. It is inferred that the power of T is determined by the dimensionality and dispersion of phonons. In BLG, since $\mu_p \sim T^{-4}$ in BG regime [101], Herring's formula $S_g \mu_p \sim T^{-1}$ is shown to be valid [64].

With regard to n_s dependence in BLG [64], $S_g \sim n_s^{-3/2}$ in the BG regime. This is in contrast with $S_g \sim n_s^{-1/2}$ in SLG [62]. This can be attributed to the different dispersion relation of the electron spectrum in BLG as in conventional 2DEG [102]. It may be inferred that, n_s dependence of S_g is determined both by the dimensionality of the electron gas and its dispersion relation. The n_s dependence of S_g suggests the possibility of tuning the magnitude of S_g in BLG by tuning n_s .

4.3. Phonon-drag thermopower in AGNR

As shown in section 3.3.3, with regard to the diffusion TEP, the geometry and edge roughness can greatly influence the TE properties of GNRs [7, 65, 88-90, 109]. A dramatic reduction in phonon transport in ZGNR [7] indicates small value for Λ . However, in an AGNR, the phonon conductance is shown to be at least one order of magnitude higher than the electronic contribution indicating a larger value for Λ in this system [110]. The role of quasi-one-dimensionality, temperature, Fermi energy and ribbon width on S_g of a semiconducting n-type AGNR is investigated by Bhargavi and Kubakaddi [100]. The Q1D electrons are assumed to interact, *via* unscreened deformation potential coupling, with the 1D acoustic phonons of frequency $\omega_q = v_s q$, wave vector $\mathbf{q} = (0, q_y)$ with the velocity v_s . The acoustic phonon energy being small, S_g in AGNR, for intrasubband ($n = n'$) transitions, can be expressed as [100]

$$S_g = -\frac{2g_s g_v |e| v_s}{L \sigma k_B T^2 \hbar^2} \sum_{n, k_y} \sum_{q_y} \hbar \omega_q |C(q)|^2 F(\theta) [\tau(E) / \rho(E)] \tau_p N_q f(E_{n, k_y}) [1 - f(E_{n, k_y} + \hbar \omega_q)] \delta(E_{n', k_y} - E_{n, k_y} - \hbar \omega_q), \quad (45)$$

where, the various quantities are already defined. In the low- T boundary scattering regime, S_g is shown to be given by [100]

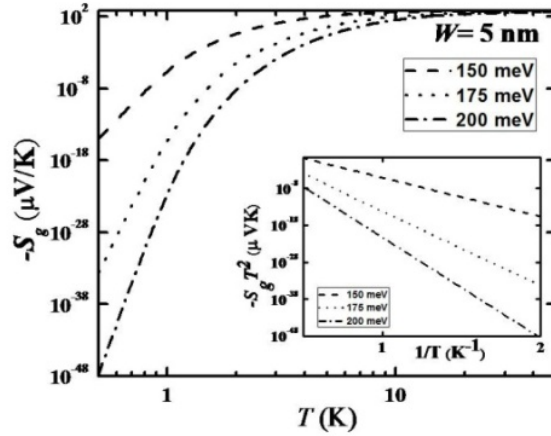


Figure 23. Phonon-drag thermopower S_g as a function of temperature T for an AGNR of width $W=5\text{nm}$ for $E_f = 150$, 175 and 200 meV. Inset: $S_g T^2$ vs $1/T$ showing an activated behavior at very low T . (from [100])

$$S_g = - \frac{D_{ac}^2 E_f \Lambda}{\pi \rho W |e| k_B T^2 (\hbar v_f)^3 (E_f^2 - E_n^2)^{1/2} v_s^2} \int_{E_n}^{\infty} \frac{g(E) E}{\rho(E) G(E) \sqrt{E^2 - E_n^2}} f(E) [1 - f(E + \hbar \omega_{q_{oy}})] (\hbar \omega_{q_{oy}})^2 N_{q_{oy}} dE \quad (46)$$

where, $E_{n,k_y} = E$, $|q_y| = |2[(k_n^2 + k_y^2)^{1/2} (v_s/v_f) - k_y]| = |q_{oy}(k_n, k_y)|$,
 $g(E) = [1 + \{E^2 + (E^2 - E_n^2)^{1/2} \hbar v_f q_{oy}\} / \{E[E^2 + 2q_{oy}(E^2 - E_n^2)^{1/2} \hbar v_f + q_{oy}^2 (\hbar v_f)^2]^{1/2}\}]/2$, and
 $G(E) = [2E(v_s/v_f) - (E^2 - E_n^2)^{1/2}] / [E_n^2 + [2E_n(v_s/v_f) - (E^2 - E_n^2)^{1/2}]^2]^{1/2}$.

In the BG regime, the energy integration in Eq.(46) gives

$$S_g \sim (1/T^2) \exp(-2\hbar v_s k_F / k_B T) \quad (47)$$

Figure 23 illustrates the temperature dependence of S_g calculated in the 1D quantum limit ($n = 1$) for $D_{ac} = 20 \text{ eV}$ [62] and $\Lambda = 10 \mu\text{m}$ [97, 98]. In the inset, a plot of $S_g T^2$ vs $1/T$ (for $T < 2\text{K}$) shows an activated behavior (Eq. (47)). At very low T , S_g is found to be exponentially suppressed, which is a new feature. This is attributed to the peculiar nature of the one-dimensional Fermi-surface consisting of discrete points. It may be mentioned here that such suppression is similar to that observed in semiconducting single wall carbon nanotubes (SWCNTs) [95, 111], but is in contrast to the well-known algebraic power laws $S_g \sim T^3$ in SLG [62] and BLG [64] and $S_g \sim T^4$ in conventional 1DEG [112]. In the high temperature region, S_g deviates from exponential behavior and finally levels off as observed in SWCNT [107, 113].

The dependence of S_g on the Fermi energy is shown in Figure 24.(a). As seen from Eq.(47), this dependence is strong unlike the case of SLG ($S_g \sim E_F^{-1}$) [62] and BLG ($S_g \sim E_F^{-3/2}$) [64]. The sensitive dependence of S_g on W is shown in Figure 24.(b). The edge roughness of AGNR modulates the phonon mean free path, which, as in SLG and BLG, significantly influences S_g . Since the ribbon edge geometry determines the electronic structure of the system, S_g in ZGNR is expected to be different from that in AGNR.

The above results in AGNR, the TEP measurements and S_g calculations in a SWNT [95, 107, 113-116], and S_g calculations in conventional 1D electron gas in semiconductor heterostructures [112, 117, 118] clearly show the importance of S_g in 1D systems.

From Eqs.(42)-(44) and (46), it may be seen that $S_g \sim \Lambda$, so that S_g may be tuned with Λ , through the sample size. Further, defining the effective phonon mean free path as $\Lambda_{eff} = \Lambda(1+p)/(1-p)$, and with specular parameter $p=0.9$ [97], S_g is shown to enhance by about an order of magnitude. For example, in BLG with $n_s = 0.5 \times 10^{12} \text{ cm}^{-2}$ at $T=10 \text{ K}$, $S_g(p=0)=0.118 \text{ mV/K}$ and $S_g(p=0.9) \approx 1.2 \text{ mV/K}$ [64].

In all the three graphene systems considered above, $S_g \sim D_{ac}^2$. In literature, the value of D_{ac} , being uncertain, is taken in the range 10-50 eV [101]. Recent measurements of resistivity [68] and hot electron energy loss rates [119] in SLG indicate the electron-acoustic phonon interaction to be unscreened. Further, a value of 19 eV for D_{ac} is found to explain well the low-T energy-loss rates, which depend only on the electron-acoustic phonon interactions. As S_g depends only upon electron-acoustic phonon coupling, unlike mobility which depends upon scattering due to other sources, detailed experimental and theoretical studies of S_g in graphene systems, particularly at low T , may also be used to determine D_{ac} .

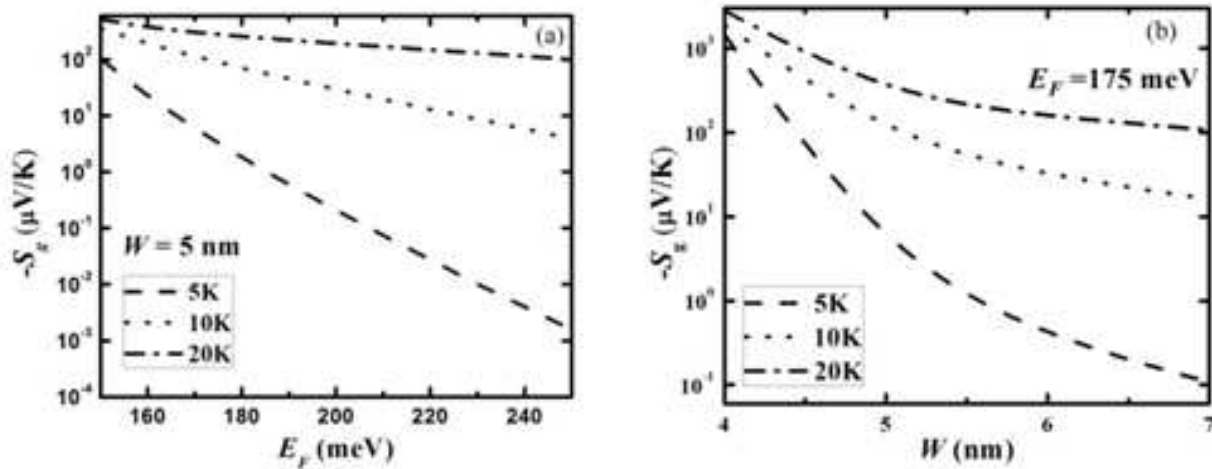


Figure 24. (a) S_g of AGNR as a function of (a) E_F with $W = 5 \text{ nm}$, and (b) W with $E_F = 175 \text{ meV}$, for $T = 5, 10$ and 20 K . (from [100])

5. Summary

In this chapter, we have reviewed the current status of the experimental investigations of the important and interesting transport property, namely TEP in graphene and described a theoretical treatment of the diffusion and phonon-drag components of TEP, in graphene systems. The treatment presented, employing the conventional Boltzmann formalism in the relaxation time approximation, gives a basic understanding of TEP in graphene systems, namely, SLG, BLG and AGNR. It gives a description of the dependences of TEP on temperature and gate bias. This understanding is expected to provide a useful guideline for improvement and optimization of performances of graphene-based TE modules.

Measurements of TEP of graphene reveal unique features not observed in metals [9] and conventional 2D semiconductor systems [10]. The graphene systems exhibit a range of TEP values up to 100 $\mu\text{V/K}$, at room temperature. The TEP changes sign across the CNP as the gate bias is varied. Away from the CNP, the TEP shows a $n_s^{-1/2}$ dependence on the carrier density n_s . At low temperatures, it exhibits a linear temperature dependence, in consonance with the Mott relation. However, a deviation from Mott formula is observed for higher temperatures.

Future experimental endeavours may aid not only in improving applicability in TE devices but also in understanding better the TE processes in graphene. Graphene may be a suitable system to realize a large range of BG regime. A detailed investigation of low-temperature (say, $T < 10$ K) TEP may enable a better analysis of the relative contributions of S_d and S_g . Exclusive data for S_g may help estimate D_{ac} . On the other hand, with proper control of S_g , the non-linear structure of S and a change in sign, exhibited in the BG regime due to S_d for smaller phonon mean free paths, may be observed. A non-linear behavior of S with a change of sign has been observed in recent experiments [120] on exfoliated SPS processed graphene. There are not many reports of measurements of TEP in BLG. Measurements of TEP of GNRs, which are awaited, can reveal the role of quasi-one-dimensionality and of the structure patterning (say, width and edge chirality) of graphene sheets. The effect of physical modifications, such as suspending and/or straining of the graphene structures, is to alter the magnitude as well as the behavior of TEP. We note that a systematic investigation of TEP as well as thermal conductivity of graphene systems is needed to describe their TE figure of merit and to get a much better understanding of scattering mechanisms operative.

Conventional low-dimensional systems, such as quantum wires and superlattices, are known to provide not only new approaches for achieving higher ZT, but also new applications such as thermal management of integrated circuits [4, 5]. The possibility of increasing ZT through engineering the electron and phonon transport, therefore, makes graphene systems attractive, in future, for applications in efficient thermoelectric devices.

Acknowledgements

This work was supported by UGC (India). The assistance of Mr. A.S. Nissimagoudar in the preparation of the manuscript is acknowledged.

Author details

N.S. Sankeshwar^{1*}, S.S. Kubakaddi¹ and B.G. Mulimani²

*Address all correspondence to: n_s_sankeshwar@hotmail.com

1 Department of Physics, Karnatak University, Dharwad, Karnataka, India

2 B.L.D.E. University, Bijapur, Karnataka, India

References

- [1] Katsnelson MI. Graphene: Carbon in Two Dimensions. Cambridge: Cambridge University Press; 2012
- [2] Castro Neto AH, Guinea F, Peres NMR, Novoselov KS, Geim AK. The electronic properties of graphene. *Rev Mod Phys* 2009; 81(1):109-62
- [3] Das Sarma S, Adam S, Hwang EH, Rossi E. Electronic transport in two-dimensional graphene. *Rev Mod Phys* 2011; 83(2):407-70.
- [4] Rowe DM., editor. Thermoelectrics Handbook - Macro to Nano. Boca Raton: Taylor and Francis; 2006
- [5] Tritt TM., editor. Recent Trends in Thermoelectric Materials Research III. Semiconductors and Semimetals Volume 71. San Diego: Academic Press; 2001
- [6] Mahan GD. Good thermoelectrics. In: Ehrenreich H. and Spaefen F. (eds.) *Solid State Physics*, vol 51, New York; Academic Press, 1998. p 81
- [7] Sevincli H, Cuniberti G. Enhanced thermoelectric of merit in edge-disordered zigzag graphene nanoribbons. *Phys Rev B* 2010; 81(11):113401-1-4..
- [8] Barnard RD. Thermoelectricity in metals and alloys. London: Taylor and Francis; 1972.
- [9] Blatt FJ, Schroeder PA, Foiles CL, Greig D. Thermoelectric power of metals. New York: Plenum Press; (1976).
- [10] Ure RW. Thermoelectric effects in III – V Compounds. In: Willardson RK and Beer AC. (eds.) *Semiconductors and Semimetals*, vol 8, New York; Academic Press, 1972. p 67-102
- [11] Gallagher BL, Butcher PN. Classical transport and thermoelectric effects in low dimensional and mesoscopic semiconductor structures. In: Landsberg PT. (ed.) *Handbook on semiconductors*, vol 1, Amsterdam; Elsevier; 1992. p.721-816.

- [12] Fletcher R. Magnetothermoelectric effects in semiconductor systems. *Semicond Sci Tech* 1999; 14(4):R1-R15
- [13] Dresselhaus MS. Quantum wells and quantum wires for potential thermoelectric applications. In: Willardson RK and Weber ER. (eds.) *Semiconductors and Semimetals*, vol 71, New York; Academic Press, 2001. p 1
- [14] Chen G. Phonon transport in low-dimensional structures. In: Willardson RK and Weber ER. (eds.) *Semiconductors and Semimetals*, vol 71, New York; Academic Press, 2001. p 203
- [15] Balandin AA. Thermal properties of graphene and nanostructured carbon materials. *Nat Mat* 2011;10(8):569–81
- [16] Zuev YM, Chang W, Kim P. Thermoelectric and magnetothermoelectric transport measurements of graphene. *Phy Rev Lett* 2009; 102(9): 096807-1-4.
- [17] Wei P, Bao W, Pu Y, Lau CN, Shi J. Anomalous thermoelectric transport of Dirac particles in graphene. *Phy Rev Lett* 2009; 102(16): 166808-1-4.
- [18] Checkelsky JG, Ong NP. Thermopower and Nernst effect in graphene in a magnetic field. *Phy Rev B* 2009; 80(20): 081413(R)-1-4.
- [19] Novoselov KS, Falko VI, Colombo L, Gellert PR, Schwab MG, Kim K. A roadmap for graphene. *Nature* 2012;490(7419):192-200
- [20] Palacios JJ, Fernandez-Rossier J, Brey L, Fertig HA. Electronic and magnetic structure of graphene nanoribbons. *Semicond Sci Technol* 2010;25(3):033003-1–10.
- [21] Bolotin KI, Sikes KJ, Hone J, Stormer HL, Kim P. Temperature-dependent transport in suspended graphene. *Phys Rev Lett* 2009; 101(9):096802-1-4
- [22] Bolotin KI, Sikes KJ, Jiang J, Klima M, Fendner G, Hone J, Stormer HL, Kim P. Ultrahigh electron mobility in suspended graphene. *Solid State Commun* 2011; 146(9): 351-55
- [23] Levy N, Burke SA, Meaker KL, Panlasigui M, Zettl A, Guinea F, Castro Neto AH, Crommie MF. Strain-induced pseudo- magnetic fields greater than 300 tesla in graphene nanobubbles. *Science* 2010;329 (5991): 544-47
- [24] Wallace PR. The band theory of graphite. *Phys Rev* 1947; 71(9):622-34.
- [25] Min H, Sahu B, Banerjee SK, MacDonald AH. Ab initio theory of gate induced gaps in graphene bilayers. *Phys Rev B* 2009; 75(15):155115-1-7.
- [26] Wakabayashi K, Takane Y, Yamamoto M, Sigrist M. Electronic transport properties of graphene nanoribbons. *New J of Phys* 2009; 11(9): 095016-1-21.
- [27] Fang T, Konar A, Xing H, Jena D. Mobility in semiconducting graphene nanoribbons: phonon, impurity, and edge roughness scattering. *Phys Rev B* 2008; 78(20): 205403-1-8.

- [28] Ochoa H, Castro E, Katsnelson MI, Guinea F. Scattering by flexural phonons in suspended graphene under back gate induced strain. *Physica E* 2012;44 (6):963-66..
- [29] Ziman JM. *Electrons and phonons*. Oxford: Clarendon Press; 1960.
- [30] Ashcroft NW, Mermin ND. *Solid state physics*. New York: Brooks/Cole; 1976.
- [31] Herring C, Geballe TH, Kunzler JE. Phonon-drag thermomagnetic effects in *n*-type germanium. I. general survey. *Phys Rev* 1958; 111(1):36-57.
- [32] Liu X, Wang D, Wei P, Zhu L, Shi J. Effect of carrier mobility on magnetothermoelectric transport properties of graphene. *Phy Rev B* 2012;86(15):155414-1-7.
- [33] Löfwander T, Fogelström M. Impurity scattering and Mott's formula in graphene. *Phy Rev B* 2007; 76(19):193401-1-4
- [34] Seol JH, Jo I, Moore AL, Lindsay L, Aitken ZH, Pettes MT, Li X, Yao Z, Huang R, Broido D, Mingo N, Ruoff RS, Shi L. Two-dimensional phonon transport in supported graphene. *Science* 2010; 328(5975):213-16
- [35] Hwang EH, Rossi E, Das Sarma S. Theory of thermopower in two-dimensional graphene. *Phy Rev B* 2009; 80(23): 235415-1-5.
- [36] Wang D, Shi J. Effect of charged impurities on the thermoelectric power of graphene near the Dirac point. *Phy Rev B* 2011; 83(11): 113403-1-4.
- [37] Jonson M, Girvin SM. Thermoelectric effect in a weakly disordered inversion layer subject to a quantizing magnetic field. *Phys Rev B* 1984; 29(4):1939-46.
- [38] Oji H, Thermomagnetic effects in two-dimensional electron systems. *J Phys C: Solid State Phys.* 1984;17(17):3059-66
- [39] Liu X, Ma Z, Shi J. Derivative relations between electrical and thermoelectric quantum transport coefficients in graphene. *Solid State Commun* 2012; 152(6):469-72.
- [40] Bonaccorso F, Lombardo A, Hasan T, Sun Z, Colombo L, Ferrari AC. Production and processing of graphene and 2D crystals. *Materials Today* 2012; 15(12):564-89.
- [41] Wu X, Hu Y, Ruan M, Madiomanana NK, Berger C, de Heer WA. Thermoelectric effect in high mobility single layer epitaxial graphene. *Appl Phys Lett* 2011; 99(13): 133102:1-3
- [42] Bergman DL, Oganessian V. Theory of dissipationless Nernst effects. *Phys Rev Lett* 2010;104(6):066601-1-4.
- [43] Ghahari F, Zuev Y, Watanabe K, Taniguchi T, Kim P. Effect of electron-electron interactions in thermoelectric power in graphene. *Bull.American Phys Soc*; 57(1) Mar2012
- [44] Puneet P, Podila R, Oleveira L, Tritt T, Rao A. Transport properties of pristine and doped graphene. *Bull.American Phys Soc*; 57(1)Mar2012

- [45] Xu X, Wang Y, Zhang K, Zhao X, Bae S, Heinrich M, Bui CT, Xie R, Thong JTL, Hong BH, Loh KP, Li B, Oezylmaz B. Phonon transport in suspended single layer graphene. arXiv:1012.2937v1 [cond-mat.mes-hall] 14Dec2010.
- [46] Babichev AV, Gasumyants VE, Butko VY. Resistivity and thermopower of graphene made by chemical vapor deposition technique. *J Appl Phys* 2013;113(7): 076101-1-3.
- [47] Sidorov AN, Sherehiy A, Jayasinghe R, Stallard R, Benjamin DK, Yu Q, Liu Z. , Wu W, Cao H, Chen YP, Jiang Z, Sumanasekera GU. Thermoelectric power of graphene as surface charge doping indicator. *Appl Phys Lett* 2011; 99(1): 013115:1-3.
- [48] Fogler MM, Guinea F, Katsnelson MI. Pseudomagnetic fields and ballistic transport in a suspended graphen sheet. *Phys Rev Lett* 2008; 101(22):226804-1-4.
- [49] Nam SG, Ki DK, Lee HJ. Thermoelectric transport of massive Dirac fermions in bilayer graphene. *Phys Rev B* 2010; 82(24): 245416-1-5.
- [50] Hwang EH, Das Sarma S. Acoustic phonon scattering limited carrier mobility in two-dimensional extrinsic graphene. *Phys B* 2008; 77(11):115449-1-6.
- [51] Wang CR, Lu WS, Lee WL. Transverse thermoelectric conductivity of bilayer graphene in the quantum Hall regime. *Phys Rev B* 2010; 82(12): 121406(R)-1-4.
- [52] Wang CR, Lu WS, Hao L, Lee WL, Lee TK, Lin F, Cheng IC, Chen JZ. Enhanced thermoelectric power in dual-gated bilayer graphene. *Phy Rev Lett* 2011; 107(18): 186602-1-4.
- [53] Xu X, Gabor NM, Alden JS, van der Zande AM, McEuen PL. Photo-thermoelectric effect at a graphene interface junction. *Nano Lett* 2010; 10(2):562-66.
- [54] Sidorov AN, Gaskill K, Nardelli MB, Tedesco JL, Myers-Ward RL, Eddy CR Jr., Jayasekera T, Kim KW, Jayasingha R, Sherehiy A, Stallard R, and Sumanasekera GU. Charge transfer equilibria in ambient-exposed epitaxial graphene on (0001) 6 H-SiC. *J Appl Phys* 2012; 111(11): 113706:1-6.
- [55] Li X, Yin J, Zhou J, Wang Q, Guo W. Exceptional high Seebeck coefficient and gas-flow-induced voltage in multilayer graphene. *Appl Phys Lett* 2012; 100(18): 183108:1-3
- [56] Sim D, Liu D, Dong X, Xiao N, Li S, Zhao Y, Li L, Yan Q, Hng HH. Power factor enhancement for few layered graphene films by molecular attachments. *J Phys Chem C* 2011; 115(5):1780-1785
- [57] Xiao Ni, Dong X, Song L, Liu D, Tay YY, Wu S, Li L, Zhao Y , Yu T, Zhang H, Huang W, Hng HH, Ajayan PM, Yan Q. Enhanced thermopower of graphene films with oxygen plasma treatment. *ACS Nano* 2011; 5(4):2749-2755.
- [58] Shaffique A, Hwang EH, Galitski VM, Das Sarma S. A self-consistent theory for graphene transport. *PNAS* 2007;104(47): 18392–18397.

- [59] Nag BR. Electron transport in compound semiconductors. Berlin: Springer-Verlag; 1980.
- [60] Ferry DK, Goodnick SM, Bird J. Transport in nanostructures. Cambridge: Cambridge University Press; 2009.
- [61] Ridley BK. Quantum processes in semiconductors. 2nd ed. Oxford: Clarendon Press; 1988.
- [62] Kubakaddi SS. Interaction of massless Dirac electrons with acoustic phonons in graphene at low temperatures. *Phy Rev B* 2009;79(7): 075417-1-6.
- [63] Vaidya RG, Kamatagi MD, Sankeshwar NS, Mulimani BG. Diffusion thermopower in graphene. *Semicond Sci Technol* 2010; 25(9): 092001-1-6.
- [64] Kubakaddi SS, Bhargavi KS. Enhancement of phonon-drag thermopower in bilayer graphene. *Phys Rev B* 2010;82(15) 155410-1-7
- [65] Nissimagoudar AS, Sankeshwar NS. Electronic thermal conductivity and thermopower of armchair graphene nanoribbons. *Carbon* 2013; 52:201-08.
- [66] Shishir RS, Chen F, Xia J, Tao NJ, Ferry DK. Room temperature carrier transport in graphene. *J Comput Electron* 2009; 8(2): 43–50 [54]
- [67] Mariani E, Oppen F. Temperature-dependent resistivity of suspended graphene. *Phys Rev B* 2010;82(19):195403-1-11.
- [68] Efetov DK, Kim P. Controlling electron-phonon interactions in graphene at ultrahigh carrier densities. *Phys Rev Lett* 2010; 105(25):256805-1-4.
- [69] Min H, Hwang EH, Das sarma S. Chirality-dependent phonon-limited resistivity in multiple layers of graphene. *Phys Rev B* 2012; 83(16):161404(R)-1-4.
- [70] Castro EV, Ochoa H, Katsnelson MI, Gorbachev RV, Elias DC, Novoselov KS, Geim AK. Limits on charge carrier mobility in suspended graphene due to flexural phonons. *Phys Rev Lett* 2010; 105(26):266601-1-4.
- [71] Sankeshwar NS, Vaidya RG, Mulimani BG. Behavior of thermopower of graphene in Bloch–Gruneisen regime. *Physica Status Solidi B* 2013; 250(7): 1356-62.
- [72] Stauber T, Peres NMR, Guinea F. Electronic transport in graphene: A semiclassical approach including midgap states. *Phy Rev B* 2007;76(20): 205423-1-10.
- [73] Bharaghavi KS, Kubakaddi SS. Scattering mechanisms and diffusion thermopower in a bilayer graphene. *Physica E* 2013; 116-21.
- [74] Li X, Borysenko KM, Nardelli MB, Kim KW. Electron transport properties of bilayer graphene. *Phys Rev B* 2011; 84(19)195453-1-5
- [75] Das Sarma S, Hwang EH, Rossi E, Theory of carrier transport in bilayer graphene, *Phys Rev B* 2010; 81(16):161407-1-4.

- [76] Peres NMR, Lopes dos Santos JMB, Stauber T. Phenomenological study of the electronic transport coefficients of graphene. *Phys. Rev. B* 2007; 76(7): 073412-1-4.
- [77] Bao WS, Liu SY, Lei XL. Thermoelectric power in graphene. *J Phys Condens Matter* 2010;22(31):315502-1-7.
- [78] Munoz E. Phonon-limited transport coefficients in extrinsic graphene. *J Phys Condens Matter* 2012; 24(19): 195302-1-8.
- [79] Sankeshwar NS, Kamatagi MD, Mulimani BG. Behaviour of diffusion thermopower in Bloch–Grüneisen regime in AlGaAs/GaAs and AlGaN/GaN heterostructures. *Physica Status Solidi B* 2005;242(14):2892-2901.
- [80] Chen W, Clerk AA. Electron-phonon mediated heat flow in disordered graphene. *Phys Rev B* 2012; 86(12): 125443-1--14
- [81] Vaidya RG, Sankeshwar NS, Mulimani BG. Diffusion thermopower in suspended graphene: effect of strain. *J Appl Phys* 2012;112(9):093711-1-6.
- [82] Vaidya RG, Sankeshwar NS, Mulimani BG. Diffusion thermopower in suspended graphene. In: Singh V, Katiyar M, Mazharier SS, Das U, Dutta A, Sodhi R, Anantharamakrishna S. (eds.) : SPIE Proceedings Vol. 8549: proceedings of the 16th national Workshop on Physics of Semiconductor Devices, IWPSD2011, 19-22 December 2011, IIT-Kanpur, India. Wahington: SPIE; 2012. doi: 10.1117/12.925343
- [83] Sharapov SG, Varlamov AA. Anomalous growth of thermoelectric power in gapped graphene. *Phs Rev B* 2012; 86(3): 035430-1-5.
- [84] Patel AA, Mukerjee S. Thermoelectricity in graphene: effects of a gap and magnetic fields. *Phy Rev B* 2012;86(7): 075411-1- 5.
- [85] Zhou B, Zhou B. Liu Z, Zhou G. Thermoelectric effect in a graphene sheet connected to ferromagnetic leads. *J Appl. Phys* 2012; 112(7):073712-1-4.
- [86] Hao L, Lee TK, Thermopower of gapped bilayer graphene, *Phys Rev B* 2010; 81(16): 165445-1-8
- [87] Divari PC, Kliros GS. Modeling the thermopower of ballistic graphene ribbons. *Physica E* 2010; 42(9):2431-2435.
- [88] Xing Y, Sun Q, Wang J. Nernst and Seebeck effects in a graphene nanoribbon. *Phys Rev B* 2009; 80(23): 235411-1-8.
- [89] Ouyang Y, Guo J. A theoretical study on thermoelectric properties of graphene nanoribbons. *Appl Phys Lett* 2009; 94(26):263107-1-3.
- [90] Karamitaheri H, Neophytou N, Pourfath M, Faez R, Kosina H. Engineering enhanced thermoelectric properties in zigzag graphene nanoribbons. *J Appl Phys* 2012; 111(5): 054501-1-9.

- [91] Zheng H, Liu HJ, Tan XJ, Lv HY, Pan L, Shi J. Enhanced thermoelectric performance of graphene nanoribbons. *Appl Phys Lett* 2012; 100(9):093104-1-5.
- [92] Mazzamuto F, Hung-Nguyen V, Apertet Y, Caer C, Chassat C, Saint-Martin J, Dollfus P. Enhanced thermoelectric properties in graphene nanoribbons by resonant tunneling of electrons. *Phys Rev B* 2011; 83(23):235426-1-7.
- [93] Lin Y, Perebeinos V, Chen Z, Avouris P. Electrical observation of subband formation in graphene nanoribbons. *Phys Rev B* 2008; 78(16):161409(R)-1-4.
- [94] Fletcher R, Zaremba E, Zeitler U. Electron-Phonon interactions in low dimensional structures. In: Challis L. (ed.) Oxford: Clarendon; 2003. p149
- [95] Tsaousidou M. Thermopower of low dimensional structures: the effect of electron-phonon coupling. In: Narlikar AV and Fu YY. (eds.) *Frontiers in Nanoscience and nanotechnology vol 2*. Oxford: Oxford University Press; 2010. p477.
- [96] Balandin AA, Ghosh S, Bao W, Calizo I, Teweldebrhan D, Miao F, Lau CN. Superior thermal conductivity of single-layer graphene. *Nano Lett* 2008;8(3): 902-07.
- [97] Nika DL, Pokatilov EP, Askerov AS, Balandin AA. Phonon thermal conduction in graphene: role of umklapp and edge roughness scattering. *Phys Rev B* 2009;79(12) 155413-1-12.
- [98] Ghosh S, Nika DL, Pokatilov EP, Balandin AA. Heat conduction in graphene: experimental study and theoretical interpretation. *New Journal of Physics* 2009;11(09) : 095012-1-19.
- [99] Cantrell DG, Butcher PN. A calculation of the phonon-drag contribution to the thermopower of quasi-2D electrons coupled to 3D phonons. *J Phys C: Solid State Physics* 1987; 20(13): 1985-2003.
- [100] Bhargavi KS, Kubakaddi SS. Phonon-drag thermopower in an armchair graphene nanoribbon. *J Phys Condens Matter* 2011;23(27):275303-1-5
- [101] Viljas JK, Heikkila TT. Electron-phonon heat transfer in monolayer and bilayer graphene. *Phys Rev B* 2010;81(24):245404- 1-9.
- [102] Fletcher R, Pudalov VM, Feng Y, Tsaousidou M, Butcher P N. Thermoelectric and hot-electron properties of a silicon inversion layer. *Phys Rev B* 1997;56(19) 12422-28
- [103] Herring C. Theory of thermoelectric power of semiconductors. *Phys Rev* 1954;96(11): 1163-1-25.
- [104] Tsaousidou M, Butcher PN, Triberis GP. Fundamental relationship between the Herring and Cantrell-Butcher formulas for the phonon-drag thermopower of two-dimensional electron and hole gases. *Phys Rev B* 2001;64(16): 165304-1-10

- [105] Tieke B, Fletcher R, Zeitler U, Henini M, Maan JC. Thermopower measurements of the coupling of phonons to electrons and composite fermions. *Phys Rev B* 1998;58(4): 2017-25
- [106] Kubakaddi SS. Effect of acoustic-phonon confinement on the phonon-drag thermopower of a two-dimensional electron gas in a semiconductor thin film. *Phys Rev B* 2004;69(03):035317-1-5
- [107] Scarola VW, Mahan GD. Phonon drag effect in single-walled carbon nanotubes. *Phys Rev B* 2002;66(20):205405-1-7
- [108] Kamatagi MD, Sankeshwar NS, Mulimani BG. Wide temperature range thermopower in GaAs/AlGaAs heterojunctions. *AIP Conf Proc.*2009; 1147:514-20.
- [109] Chen Y, Jayasekera T, Calzolari A, Kim KW, Nardelli MB. Thermoelectric properties of graphene nanoribbons, junctions and superlattices. *J Phys Condens Matter* 2010;22(37):372202-1-6
- [110] Mazzamuto F, Hung Nguyen V, Nam DV, Caer C, Chassat C, Saint-Martin J, Dollfus P. In: proceedings of 14th International workshop on computational electronics p 1-4, IWCE, Pisa, IEEE Xplore; 2010.
- [111] Tsaousidou M. Theory of phonon-drag thermopower of extrinsic semiconducting single-wall carbon nanotubes and comparison with previous experimental data. *Phys Rev B* 2010;81(23):235425-1-9
- [112] Kubakaddi SS. Electron-phonon interaction in a quantum wire in the Bloch-Gruneisen regime. *Phys Rev B* 2007;75(7) 075309-1-7
- [113] Vavro J, Llaguno MC, Fischer JE, Ramesh S, Saini RK, Ericson LM, Davis VA, Hauge RH, Pasquali M, Smalley RE. Thermoelectric power of p-doped single-wall carbon nanotubes and the role of phonon drag. *Phys Rev Lett* 2003;90(06):065503-1-4
- [114] Zhou W, Vavro J, Nemes NM, Fischer JE, Borondics F, Kamarás K, Tanner DB. Charge transfer and Fermi level shift in p-doped single-walled carbon nanotubes. *Phy Rev B* 2005;71(20): 205423-1-7.
- [115] Yu C, Shi L, Yao Z, Li D, Majumdar A. Thermal conductance and thermopower of an individual single-wall carbon nanotube. *Nano Lett* 2005;5(9):1842-46
- [116] Tsaousidou M. Phonon-drag thermopower of ballistic semiconducting single-wall carbon nanotubes and comparison with the semiclassical result. *Europhysics Lett* 2011;93(4) 47010-1-8
- [117] Kubakaddi SS, Butcher PN. A calculation of the phonon-drag thermopower of a 1D electron gas. *J Phys Condens Matter* 1989;1(19):3939-46
- [118] Tsaousidou M, Butcher PN. Phonon-drag thermopower of a ballistic quantum wire. *Phys Rev B* 1997;56(16):R10044-10047

- [119] Baker AMR, Alexander-Webber JA, Altebaeumer T, McMullan SD, Janssen TJBM, Tzalenchuk A, Lara- Avila S, Kubatkin S, Yakimova R, Lin C-T, Li L-J, Nicholas RJ. Energy loss rates of hot Dirac fermions in epitaxial, exfoliated and CVD graphene. *Phys Rev B* 2013;87(04):0454014-1-6
- [120] Rao A. Private communication 2012.

IntechOpen

IntechOpen

